7-2014

Springtime Atmospheric Responses to North Atlantic SST Anomalies in Idealized GCM Experiments: Northern Hemisphere Circulation and North American Precipitation

Michael C. Veres
University of Nebraska-Lincoln, michael.veres@yahoo.com

SPRINGTIME ATMOSPHERIC RESPONSES TO NORTH ATLANTIC SST ANOMALIES IN IDEALIZED GCM EXPERIMENTS: NORTHERN HEMISPHERE CIRCULATION AND NORTH AMERICAN PRECIPITATION

by

Michael C. Veres

A DISSERTATION

Presented to the Faculty of
The Graduate College at the University of Nebraska
In Partial Fulfillment of Requirements
For the Degree of Doctor of Philosophy

Major: Earth and Atmospheric Sciences
(Meteorology/Climatology)

Under the Supervision of Professor Qi Hu

Lincoln, Nebraska

July, 2014

SPRINGTIME ATMOSPHERIC RESPONSES TO NORTH ATLANTIC SST ANOMALIES IN IDEALIZED GCM EXPERIMENTS: NORTHERN HEMISPHERE CIRCULATION AND NORTH AMERICAN PRECIPITATION

Michael C. Veres, Ph.D.

University of Nebraska, 2014

Adviser: Qi Hu

In this study, a series of experiments using idealized sea surface temperatures (SST), land and orography are performed to examine the interactions between the Atlantic Multidecadal Oscillation (AMO), continents and major orography. Three sets of experiments are done using an increasingly realistic surface boundary (aqua-planet, land without orography and land with orography) and run using perpetual equinox conditions. For each land surface boundary, the model is forced with a zonally symmetric SST, with additional experiments with an imposed positive or negative SST anomalies in the North Atlantic. The experiments are then compared to determine how these forcings interact and what factors may contribute to the observed atmospheric responses to the AMO.

It was found that there are strong nonlinearities in how the atmosphere responds to the warm and cold North Atlantic SST anomalies. During the warm phase of the AMO (warm SST anomaly), there are strong responses in circulation in the Northern Hemisphere and precipitation over North America. When continents are included in the model, these responses are generally enhanced. Orography, on the other hand, acts to weaken the previous forced responses. In contrast, the mid-latitude response during the cold phase of the AMO (cold SST anomaly) is far weaker. We found that land still forces

strong mid-latitude responses in both circulation and North American precipitation. However, orography offsets the effects of the land, further altering the response pattern to the cold SST anomaly. These complex interactions between the SST anomalies, land and orography act to produce the generally weak springtime patterns shown in previous studies about the AMO. Furthermore, the modeled details of land and orography interactions and their effects on the responses to the SST anomalies allow for a better understanding of how observed patterns in the AMO responses develop and what may cause variations of those responses.

Acknowledgements

I would like to thank my dissertation adviser, Dr. Qi Hu, for helping to guide me through the research presented in this dissertation. I would also like to thank my committee members, Drs. Robert Oglesby, Song Feng and Clinton Rowe for graciously agreeing to be members of my committee. Additionally, I would like to thank Drs. Oglesby and Rowe for their editorial comments. This research would not have been possible without the use of University of Nebraska-Lincoln's Holland Computing Center and the NCAR Bluefire and Yellowstone (http://n2t.net/ark:/85065/d7wd3xhc) computing systems. Funding was provided by NOAA Grant NA09OAR4310188 and NSF Grant AGS-1103316. I would also like to thank the current and past members of Bessey 132 (Rebecca Duell, Sabrina Jauernic, Mengyuan Shang and Qianru Wu) for putting up with me and going along with my insanity as I worked on this dissertation, particularly near the finish. My family provided much support through my time in graduate school (and before) and I would like to thank them for all that they have done for me. Finally, I would like to thank Megumi Watanabe for being there when I needed someone to talk to and for helping get me through the toughest times.

Table of Contents

List of Figures

List of Tables

CHAPTER 1

INTRODUCTION

Spring and summer rainfall accounts for the majority of precipitation in the Great Plains of the United States. Variations in precipitation during the spring and summer can lead to flooding or drought, therefore it is apparent that a better understanding of the forcings behind precipitation variations would be beneficial. Many processes, local and remote, have been shown to impact precipitation in the central U.S. It can be argued that any variability in either the forcing processes or interactions between multiple local and remote processes can potentially alter precipitation. As such, a better understanding of the precipitation and circulation responses to individual forcings is needed. Furthermore, we need to better understand how these forcings can individually produce variations in precipitation and how they may interact. Increased understanding of these interactions can allow for better climatic predictions of circulations and precipitation.

Several major forcings have been found to be important in accounting for variations in spring and summertime precipitation in the central U.S. One local forcing is the Great Plains Low-Level Jet (GPLLJ) that flows from the Gulf of Mexico into the central U.S. The GPLLJ brings large amounts of moisture into the central U.S. and is known to be a significant factor in warm-season precipitation development (Higgins et al. 1997; Wang and Chen 2009). The transport of moisture can sometimes be augmented by the local factors, such as soil moisture content (Schubert 2004; Oglesby and Erickson 1989; Oglesby et al. 2001; Veres and Hu 2013). Other remote forcings, notably variations in sea surface temperatures (SST), have been shown to have a strong impact on

precipitation in the central U.S., by modifying the large- and regional-scale circulations and the GPLLJ. A primary source of remote SST forcing is the El Niño-Southern Oscillation (ENSO), which has been found to strongly impact summertime precipitation in the central U.S. (Hu and Feng 2001; Mo et al. 2009). Meanwhile, variations in North Pacific SST from the Pacific Decadal Oscillation (PDO; Ting and Wang 1997; Wang et al. 2010) and North Atlantic SST from the Atlantic Multidecadal Oscillation (AMO; Enfield et al. 2001; Wang et al. 2010; Hu et al. 2011) appear to have similar remote effects on U.S. precipitation. Finally, some studies have started to look at the combined effects of some of these forcings (Mo et al. 2009; Hu and Feng 2012), but the interactions of the forcings have been studied to a much lesser extent than the individual forcings have been.

In the present study, we are interested in how the AMO impacts the global circulation and North American precipitation. For reference, the AMO is a 60-80 year cycle in North Atlantic SST anomalies (Enfield et al. 2001; Fig. 1.1) driven by heat and salinity changes in the Atlantic Meridional Overturning Circulation (AMOC; Wang and Zhang 2013). During the warm phase of the AMO, the North Atlantic SSTs are warmer than average. The reverse is true in the cold phase of the AMO, which has colder than normal SSTs. Though the observational record only extends into the mid-19th century, proxy data have been used to identify AMO-like patterns globally over the previous two millennia (Feng and Hu 2008; Gray 2004; Poore et al. 2009).

In the following discussion, we include some results from previous work for summer. While this study is focused on springtime circulations and precipitation, there has been far less work done on the springtime atmospheric responses than there has been

on the summertime responses. Therefore, we include some information from previous studies about the atmospheric response during summer to provide additional background on the relationship between the AMO and warm season precipitation.

Previous work has shown an often inconsistent connection between the AMO and warm season precipitation in the central U.S. The general consensus among previous studies is that in the central U.S., the warm (cold) phase of the AMO forces weaker (stronger) precipitation. McCabe et al. (2004) found that the AMO forces 28% of the variability in central U.S. droughts. This agrees with other studies that found that warm season precipitation decreases during the warm phase of the AMO (Hu and Feng 2008; Feng et al. 2010; Hu et al. 2011; Wang et al. 2010). However, the mechanisms proposed that connect central U.S. precipitation and the AMO vary considerably between studies. As an example, both the modeling results by Hu et al. (2011) and the principle component analyses of Nigam et al. (2011) indicate fairly strong and robust decreases in summertime precipitation during the warm phase of the AMO in the continental U.S., with the exception of the desert southwest and Florida. On the other hand, the modeling study of Wang et al. (2010), based on the rotated empirical orthogonal functions of Schubert et al. (2009), limits the region of reduced precipitation to the Great Plains and mountains west of the Mississippi River. East of the Mississippi River and along the coast of the Gulf of Mexico, their analysis yields regions with considerable increases in precipitation.

During the cold phase of the AMO, studies do not indicate a robust signal in the U.S. precipitation anomalies. Wang et al. (2010) show few notable precipitation anomalies during spring and while the anomaly magnitudes increase in the summer, the

signs of the anomalies are mixed. In the summer, the Great Plains and Midwest have increased precipitation, whereas precipitation in the south is decreased. This contrasts with the results of Hu et al. (2011), who showed that the southern U.S. and parts of the Great Plains have increased precipitation and the Midwest generally has reduced precipitation during the cold phase of the AMO.

These inconsistencies suggest that the response to the AMO is complex. One source of the weak and/or inconsistent anomalies shown in other studies may be nonlinear interactions of AMO-forced circulation responses with other forced responses in the atmosphere. Two such forcings that are always present are the continental land-masses, and major orographic features. Both forcings are well known to alter atmospheric circulations significantly, particularly in the Northern Hemisphere (e.g., Peixoto and Oort 1992). One way in which land and orography alter the circulation is by forcing asymmetries in the zonal distributions of diabatic heating. Zonal asymmetries in both sensible heating (Derome and Wiin-Nielson 1971) and latent heat release (Ting 1994) help drive these circulation asymmetries. Direct mechanical forcing from the mountains are also major modifiers of global circulations (Derome and Wiin-Nielson 1971). These forcings act to create standing waves in the time-mean circulations which serve to alter the circulations well beyond the mountain region. Considering the ever-present nature of these forcings, it is highly likely that they interact with any AMO-forced circulations and influence the observed response to the AMO SST anomalies. Ultimately, these interactions produce the circulation and precipitation anomalies seen in observations and simulated in models. The *direct* response to the AMO is not itself seen in reality or in the realistic model simulations, as it is always modified to some extent by

the other forcings that are always present. Presumably, these modifications of the atmospheric response to the SST anomalies likely complicate the responses to the AMO found in previous studies.

If the land and orography forcings are always present then, why is there a need to determine the direct response to the AMO SST anomalies when it would be unlikely to be observed in reality? In short, the land and orography forcings can potentially be variable and there is potential for the interactions between land and orography, and the SST anomalies to be altered as a result. Ringler and Cook (1999) suggested that circulation patterns (i.e., standing waves) forced by orography can vary inter-annually, potentially from year-to-year variations in soil moisture, snow cover, and land use and alterations in the diabatic heating rate at the surface. When this occurs in mountainous regions, the change in heating can alter the structure of the standing waves forced by orography. A similar process likely occurs over non-orographic regions as well. Drought decreases soil moisture and vegetation health (Breshears et al. 2005), leading to the widespread death of vegetation. These factors can lead to increases in the surface heating rate by altering the Bowen ratio (ratio of sensible to latent heat flux at the surface), due to the decreased soil moisture content, or by changes in albedo in response to vegetation die-off. Similar processes can be expected to occur in response to excess precipitation. When these occur on a continental or sub-continental scales, it is reasonable to assume that large-scale alterations to the circulation patterns forced by the land masses can occur.

Due to these modifications by land and orography on the AMO-forced response and the potential for variations in those modifications, it is apparent that a better

understanding of the individual forcings and their interactions with one another is needed. In the studies by Hu et al. (2011), Wang et al. (2010), Mo et al. (2009), and others, a fully-realistic surface boundary was used in addition to AMO-like SST anomalies. However, these studies only examined the sum total of the direct forcings and, indirectly, their interactions. Not much is known about the direct atmospheric response to the AMO or how it is modified by land and orography. This motivates the need for a modeling study in which the atmospheric responses to individual forcings and their interactions can be separately examined.

In this study, we use a general circulation model (GCM) to gain a better understanding of the direct atmospheric responses to North Atlantic SST anomalies and also how those responses may be modified by the presence of land and orography. To do this, we perform a series of experiments using idealized surface boundaries, SST anomalies, but a fully dynamic atmosphere. In the first set of experiments, an aqua-planet (all-ocean) surface boundary is used, with warm or cold SST anomalies placed at the latitudes and longitudes of the North Atlantic. The SST anomalies used in this study differ some from the realistic AMO, as it was attempted to keep the anomaly as simple as possible. However, the anomaly gives an approximate response to AMO-like SST anomalies that are free from alterations due to land and orography. For a detailed description of aqua-planet simulations, please see Blackburn et al. (2013) and references therein. To determine how land modifies the atmospheric response to the SST anomalies, we include idealized continents without orography. By examining the differences between the aqua-planet and idealized continent simulations, we can determine the extent of any modifications due to land vs. just the ocean on the atmospheric response to North

Atlantic SST anomalies. The third and final level of complexity involves adding idealized orography to the land surface. These results can then be compared to the land without orography experiments to determine how orography can further modify the atmospheric response to the AMO. This addition of orography creates a land surface that is more comparable to reality and allows for more direct comparisons between the current study and more realistic simulations, as well as observations. Through comparisons with more realistic studies and the details of the direct and modified responses, we hope to gain a better understanding of the circulation and precipitation anomalies forced by the AMO.

To this end, we take a similar approach as in Brayshaw et al. (2008, 2009, 2011), who examined the direct responses to North Atlantic SST anomalies, idealized land and orography (Rocky Mountains only) and, to some extent, their interactions. While the studies by Brayshaw et al. (2008, 2009, 2011) provide good insight into the circulation, precipitation and storm track responses to these forcings, unfortunately there is relatively little discussion about the interactions between topography and the SST anomalies. Therefore, we expand upon the designs and goals of their studies. In particular, we focus on the interactions between the forcings and use SST anomalies similar to the AMO. We also expand upon their orography experiments by including the Alps and Tibetan Plateau, in addition to the Rocky Mountains. Other orographic features beyond the Rocky Mountains have been found to be important forcings on Northern Hemisphere circulation (Broccoli and Manabe 1992). Specifically, the Tibetan Plateau has been shown to have a strong influence on North American circulation due to upstream diabatic heating (Ting 1994). It is the aim of the current study to expand upon their work and to understand

how these forcings interact and modify one another to produce the observed response to the AMO.

We choose to use idealized representations of land and orography because of the ability of land surface heterogeneities to force local- and regional-scale variations in circulations. In particular, Pielke Sr. (2001) found that spatial variations of land surface types can force regional zones of convergence and convection. Differences in soil moisture, soil type, surface roughness, albedo and other surface parameters alter the land-atmosphere interaction by introducing spatial inhomogeneities in the surface energy budgets (Chase et al. 1999; Pielke Sr. et al. 2007). The primary reason for this spatial variability in energy is from a change in the partition between the latent and sensible heat fluxes, leading to increased or decreased surface heating rates (Chase et al. 1999; Pielke Sr. 2001). Furthermore, Pielke et al. (1991) found that moderately large surface heterogeneities of around 80 km can force vertical motions that, under certain conditions, can transport heat into the middle troposphere. It is reasonable to assume that these regional-scale circulations and energy transports can interact with AMO-forced circulations and alter the local responses. In addition to altering the direct response to the AMO, it is likely that these circulations would also alter any modified responses forced by land and orography as well. These potential alterations from land heterogeneity make it imperative to have the simplest land and orography possible to limit any additional forcings that can complicate the atmospheric responses.to the AMO. While this somewhat limits the extent to which this study can be compared to more realistic studies, the current study is focused on the direct response to the AMO and the large-scale

modifications by land and orography. Any regional-scale alterations can potentially mask these essential responses.

In Chapter 2, we provide details of the model used in this study and the specifics for the experiment design. Chapter 3 details the general circulation responses from the series of experiments using simplified surface boundaries (aqua-planet, idealized land and orography). Chapter 4 examines the impact of these circulation responses on precipitation over North America. Conclusions and potential implications of this work are provided in Chapter 5.

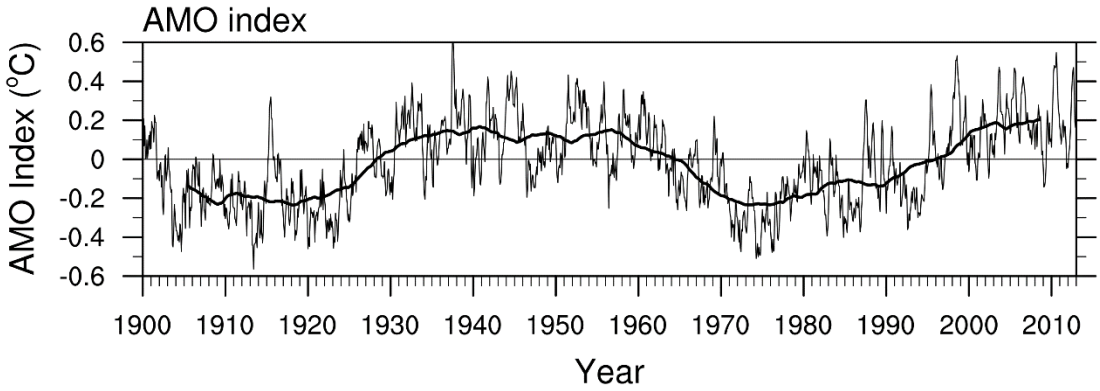

Figure 1.1: Time-series of the AMO index since 1900 (Enfield et al. 2001). Thin line is the unsmoothed monthly data and the heavy line is an 11-year running average. Data are obtained from the Earth System Research Lab (http://www.esrl.noaa.gov/psd/data/timeseries/AMO/).

CHAPTER 2

MODEL DESCRIPTION AND EXPERIMENT METHODOLOGY

2.1 Model Description

We used the National Center for Atmospheric Research (NCAR) Community Earth System Model version 1.0.5 (CESM1.0.5) for this study (Hurrell et al. 2013). The CESM includes component models for the atmosphere, land and ocean as well as land and sea ice. Specifically, we used the Community Atmospheric Model version 5.1 (CAM5.1) coupled to the Community Land Model version 4 (CLM4). To keep the experiments as simple as possible and to eliminate additional forcings, the other component models are not actively used in this study. The horizontal resolution for CAM5.1 and CLM4 used in this study is a spectral resolution of T85, which is then output on a 1.4°×1.4° latitude and longitude grid. The CAM4 physics package is used in this study and has 26 vertical levels. Its use was necessitated primarily by the need for prescribed aerosols (CAM5 only had prognostic aerosols). CLM4 is run mostly in its standard, default mode; modifications to both CLM4 and CAM5.1 will be detailed later in this chapter. Sea surface temperatures (SST) are prescribed using analytical equations, and sea ice is prevented from forming. The land ice (glacier) model is prevented from running, although the land model does produce a modest sized snowpack in the high latitudes (generally north of 55°N).

2.2 Experiment Design and Model Settings

Numerous changes to the model and input files were needed to produce the idealized conditions with minimal external/additional forcings. We utilized many of the resources available from the NCAR Paleoclimate Working Group (PWG), which included the Paleo User's Guide and Paleo Toolkit available through the PWG website (http://www2.cesm.ucar.edu/working-groups/pwg).

As shown in Table 2.1, nine model experiments were made in this study; all of which run under perpetual spring equinox conditions. Running the model under the perpetual conditions allows for the model to reach equilibrium so a steady-state solution can be determined. Additionally, running the model under perpetual conditions allows for every month to be used in the analysis of a single season, thereby extending the effective length of the integration. This would not be possible if transient (time-varying) conditions were used. Choosing perpetual equinox conditions also prevents excessive cooling (heating) in the winter (summer) hemisphere due to weak (strong) solar insolation.

Each experiment was run for 20 years and reached equilibrium within the first year. We use years 3-20, discarding the first two years as spin-up and only examining the steady-state solution. Though equilibrium was reached fairly quickly, the second year was discarded in order to be cautious and not introduce any irregularities into the time-mean and variance calculations.

In order to allow for the model to reach a steady-state equilibrium, all transient forcings were removed. They included, but were not limited to, setting all three orbital forcings to zero (forcing a perfectly circular orbit and an axial tilt of 0°) and solar

insolation was held at 1365 W/m^2. Aerosol and volatile organic compound emissions were also set to zero and there was no time variation in the vegetation. To limit the effect of forcings from a heterogeneous land surface, the land surface type was set to cool grassland. Finally, the potentially extensive impact from atmospheric aerosols was eliminated by setting all prescribed aerosols to be zero.

The simplest surface boundary we use is an aqua-planet (all-ocean) boundary (Fig. 2.1a). The zonally symmetric (control) SST is derived from the QOBS distribution, which was initially described in Neale and Hoskins (2000) and later modified by Brayshaw et al. (2008). The QOBS analytical solution is zonally symmetric and only a function of latitude. Modifications to the QOBS solution in the current study were made to get better agreement with the observed global SST during an equinox. To determine an approximate SST pattern for the equinox, we used the Hadley Centre HadSST2 (Rayner et al. 2006) climatology dataset for March, from 1961-1990. March was selected, instead of September, because we wanted to avoid the strong heating from boreal summer that is still present in September (Peixoto and Oort 1992). The global SST for March were zonally averaged and then the Northern and Southern Hemispheres were averaged to obtain a representative SST pattern for the equinox. Because of this process, the results in this study are more representative of boreal spring than fall. Figure 2.2 shows the observed and analytical SSTs. The analytical SST solution is given by

$$\mathrm{SST}(\phi) = \frac{T_{max}}{2}\left[2 - \sin^4\left(\frac{18\phi}{13}\right) - \sin^2\left(\frac{18\phi}{13}\right)\right] \qquad (2.1)$$

Where, T_{max} is the maximum SST (28°C) and occurs along the equator, and ϕ is the latitude. SST from (2.1) goes to zero at 65° latitude, 5° closer to the pole than the original equation of Neale and Hoskins (2000). Poleward of 65° latitude, SST was set to

0°C, preventing sea ice (which forms at -1.8°C). As shown in Fig. 2.2, the analytical solution is relatively consistent with the observed zonal average SST. The most notable difference between the two are in the subtropics and tropics. While it is possible to get better agreement in the low latitudes by increasing T_{mas}, this would weaken the agreement in the mid-latitudes. Considering that the SST anomalies of the AMO are largely and mid- and high-latitude phenomena, it was determined that the mid-latitude SST pattern should be as accurate as possible.

For the SST anomaly experiments, we impose a monopole perturbation in the Northern Hemisphere onto the zonally symmetric SST distribution in (2.1). The perturbation equation is inspired by Brayshaw et al. (2008) and is given by

$$\Delta SST(\phi, \lambda) = \Delta T_{max} \cos\left[\pi\left(\frac{\lambda-\lambda_o}{\Delta\lambda}\right)\right] \cos^2\left[\pi\left(\frac{\phi-\phi_o}{\Delta\phi}\right)\right] \qquad (2.2)$$

In (2.2), ΔT_{max} is the SST anomaly maximum (±4°C), λ, λ_o and $\Delta\lambda$ are the longitude, central longitude and longitudinal radius of the anomaly, respectively, ϕ, ϕ_o and $\Delta\phi$ are the same, but for the latitude. The anomaly is centered at 35°N latitude, 40°W longitude, and has 30° radius in both latitude and longitude. Figure 2.1 shows the extent of the SST anomaly as concentric circles in the North Atlantic. It should be noted that the prescribed SST anomaly is several times stronger than the observed SST anomaly forced by the AMO. This was made to increase the signal-to-noise ratio in the model response.

In the idealized land experiments, three continents were included; North America, South America and Eurasia (Fig. 2.1b). All three continents are simple geometric shapes and have an elevation of 1 meter above sea level to limit any effect of orography on the atmosphere. The land model (CLM4) was run as a fully dynamic model, with no restrictions on land temperatures, soil moisture or other time-variant

parameters. Vegetation type was constant and there was no temporal variance in any vegetation parameters. However, the land itself was homogeneous to limit any spatial variations that force local- or regional-scale circulations. Only a single land surface type was used (cool grassland), soil is homogenous, and there were no rivers or coastal irregularities. In the experiments with a SST anomaly, the perturbation was not smoothed or otherwise changed and is truncated at the coastlines of the continents.

The land model and input files required additional modifications beyond the setting of the continental boundaries and surface parameters (i.e., land surface type). First, the River Transport Model (RTM) in CLM4 was turned off, as there are no rivers on the idealized continents. There was also an issue with the continental boundaries due to the interpolation of the land data. The initial land surface data were created on a 0.5°×0.5° latitude and longitude grid (out of requirement from the PWG toolkit) and then interpolated onto the T85 Gaussian grid. As a result, there were grid points of excessively small land fractions and this created a fault in the Zhang-McFarlane (Z-M) convection scheme in CAM5.1. This necessitated forcing land cells with small land fractions to become a water cell. A minimum value of 1% land fraction in the interpolated land data was chosen to the threshold for a land cell. Grids with a smaller percentage were changed to water.

For the experiments with orography, modified Gaussian shapes were used to represent idealized versions of the Rocky Mountains, Alps and the Tibetan Plateau (Fig. 2.1c). Despite their importance, the Andes were not included in the model, as their impact in the Northern Hemisphere would likely be smaller compared to the major orography in the Northern Hemisphere. This methodology is similar to Brayshaw et al.

(2009). The heights, shapes and orientations of the mountains were chosen to be relatively well representative of the realistic orographic features. For all three orographic features, only the elevation of the land is changed. There were no modifications made to the land surface type or other surface parameters when the mountains are included. Care was taken to ensure that the orography was restricted to the land and that there were no "water mountains."

The basic function for the orographic shapes is a 2-dimensional Gaussian function and is given by

$$f(\phi,\lambda) = A \exp\left[-\left(\frac{(\lambda-\lambda_o)^2}{2\sigma_\lambda^2} + \frac{(\phi-\phi_o)^2}{2\sigma_\phi^2}\right)\right] \quad (2.3)$$

In (2.3), λ and ϕ are the longitude and latitude, respectively, and λ_o and ϕ_o are the central longitude and latitude. σ_λ and ϕ_y are the longitudinal and latitudinal half-widths (i.e., standard deviation) of the function. The specific values for each orographic feature are included in Table 2.2.

After the basic function is defined for each orographic feature, further modifications were made. For the Tibetan Plateau, all elevations greater than 4500 meters above the sea level were truncated to that elevation, producing a plateau of realistic size and shape. Several modifications were made for the Rocky Mountains as well. The first is related to the fact that the Rockies are not oriented completely meridionally, but slant from southeast to northwest. As a result, the idealized Rockies are rotated 30° counter-clockwise to better represent their realistic orientation. The Gaussian shape was then elongated, producing a major-axis and better simulating the realistic extent of the high mountains of the Rockies. Additionally, the smaller size of North America compared to Eurasia requires that the tail of the Gaussian shape be shortened

(elevations less than 50m). Without this step, the Rockies extend over water and small water mountains form near the coastlines. To avoid this from happening, areas with elevations less than 10 meters above the sea level are set to be at sea level (0 meters), and then the elevations between 10 and 50 meters above sea level were scaled accordingly to prevent a cliff edge around the mountains. A similar procedure was performed for the Alps, but without the rotation, and the Alps were elongated along their latitudinal (east-west) axis.

2.3 Model Modifications

While most of the changes needed to run these experiments were made by modifying the input data, one modification to the model source code was required. The partial pressure due to dry air at the surface (i.e., dry air mass) in CAM5.1 is coded directly into the model and is based on the realistic topography. In order to be able to make direct comparisons between the different surface boundaries, a correction to the dry air partial pressure must be made for each surface boundary. However, no changes were made to the partial pressure of water vapor (i.e., the moist air mass) and it was left at 2.45 hPa for all experiments.

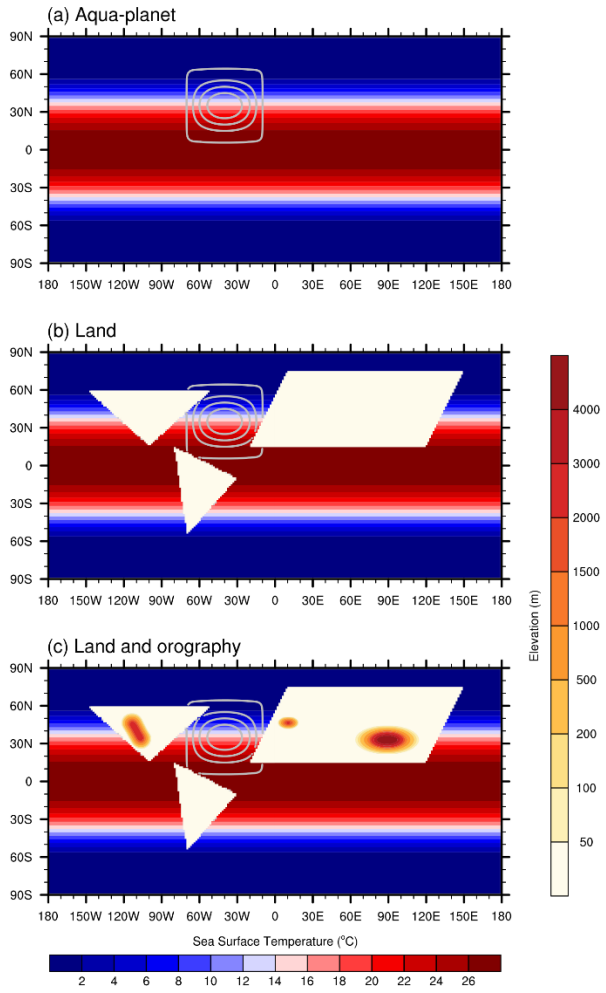

Figure 2.1: SST and topography distributions for the (a) aqua-planet, (b) land without orography and (c) land with orography experiments. Concentric circles in the North Atlantic indicate the location and intensity of the SST anomalies in the warm and cold SST anomaly runs. Outermost contour is 0°C and then they increase or decrease by 1°C, reaching ±4°C at the center.

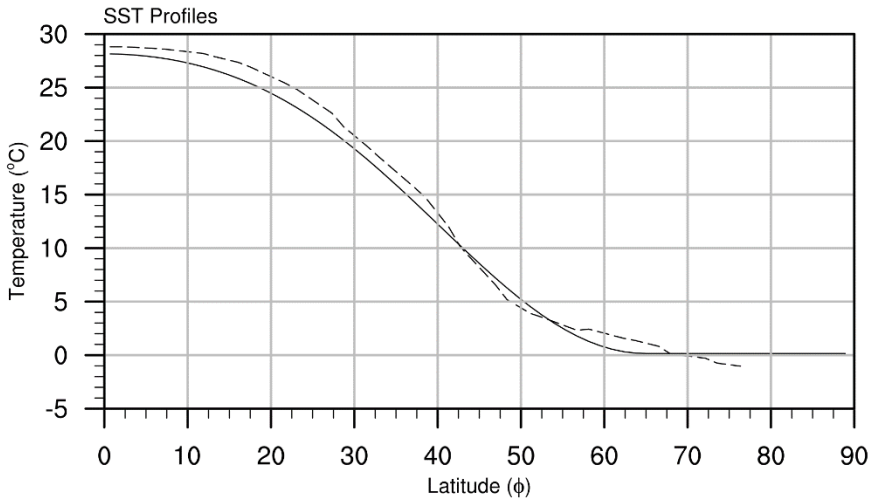

Figure 2.2: Figure showing the (a) analytical SST (solid line) and the (b) Hadley Centre's time and zonal average SST for March, 1961-1990 (HadSST2; Rayner et al. 2006; dashed line). For (b), the Northern and Southern Hemispheres are averaged to produce representative equinox conditions.

Table 2.1: Summary of the experiments used in this study. The land experiments include idealized representations of Eurasia, North America and South America. Orography consisted of idealized representations of the Rocky Mountains, Alps and the Tibetan Plateau.

	Topography		
SST	Continents	Orography	Description
Control	No	No	Aqua-planet, zonally symmetric (control) SST
Cold	No	No	Aqua-planet, control SST w/negative anomaly in the North Atlantic
Warm	No	No	Aqua-planet, control SST w/positive anomaly in the North Atlantic
Control	Yes	No	Idealized land, control SST
Cold	Yes	No	Idealized land, control SST w/negative anomaly in the North Atlantic
Warm	Yes	No	Idealized land, control SST w/positive anomaly in the North Atlantic
Control	Yes	Yes	Idealized land and orography, control SST
Cold	Yes	Yes	Idealized land and orography, control SST w/negative anomaly in the North Atlantic
Warm	Yes	Yes	Idealized land and orography, control SST w/positive anomaly in the North Atlantic

Table 2.2: Table summarizing the parameters used in the Gaussian functions that produced the idealized orography.

Parameter	Orographic feature			Description
	Rocky Mountains	Alps	Tibetan Plateau	
A	3000 meters	4000 meters	7500 meters	Amplitude of the function
x_o	110°W	10.5°E	89°E	Central longitude
y_o	40°N	46.5°N	33°N	Central latitude
σ_x	≈ 2.7386°	≈ 1.1180°	≈ 7.9057°	Longitudinal half-width
σ_y	≈ 2.7386°	≈ 1.1180°	≈ 3.5355°	Latitudinal half-width

CHAPTER 3

GENERAL CIRCULATION RESPONSE

3.1 Direct Response to the Aqua-planet Control SST

The mean circulations from the aqua-planet experiment with the control (i.e., zonally symmetric) SST provide a base state from which we examine the more complex simulations with SST anomalies, lands and topography. Examination of the aqua-planet experiment using a symmetric SST also provides a test and validation of the modifications made to the model. If we consider the extent of the surface boundary modifications in the model, it is important to know that the model responds reasonably to the highly altered boundary conditions. In the absence of asymmetrical forcings, the control response should be zonally symmetric and an idealized version of the well-known general circulation patterns (e.g., Peixoto and Oort 1992). Figure 3.1 shows the geopotential heights at 850 and 200 hPa. It is apparent that the responses at both pressure levels are zonally symmetric and are consistent with an unmodified meridional circulation. A subtropical high pressure belt between 20°-30°N at 850 hPa (Fig. 3.1a) is indicative of a zonally symmetric subsiding branch of the Hadley Cell circulation. The winds in the lower troposphere are also geostrophic, which is also consistent with the weaker surface friction from the lack of topography. Though not easily apparent in Fig. 3.1, the Inter-tropical Convergence Zone (ITCZ) occurs along the equator and separates two distinct Hadley circulations, one in each hemisphere.

As expected, the geopotential heights at 200 hPa are determined by the equator to pole temperature gradient and is also zonally symmetric (Fig. 3.1b). The greatest heights

are found in the tropics and the lowest heights are found in the high latitudes, a pattern consistent with the global meridional heating distribution. Stronger winds occur aloft and are also geostrophic, with the exception being in the tropics. Here, there is a notable northward (i.e., ageostrophic) component to the wind produced by the upper branch of the Hadley circulation.

Similarities between the circulations in Fig. 3.1 and general circulation theory indicate that the model handles the altered surface boundary conditions appropriately. The basic circulation shown in Fig. 3.1 is quite useful in creating a context for the responses to more complex model configurations with SST anomalies in the North Atlantic Ocean, and the lands and orography.

3.2 Responses to Warm and Cold SST Anomalies in the Aqua-planet

After the basic response to the control SST is known, we can add the warm and cold SST anomalies to the aqua-planet. Previous studies using an aqua-planet have shown the importance of diabatic heating on forcing atmospheric circulations and standing waves (Webster 1981, 1982). As such, we begin with an analysis of the diabatic heating anomalies in the atmosphere in response to the warm and cold SST anomalies. Diabatic heating is composed of the sensible and latent heats. Sensible heating generally contributes less to the overall heating rate, with latent heating from condensation being far greater (Ting 1994). We calculate the latent heating anomalies from the precipitation anomalies (by assuming that all energy released from condensation occurs at the same location as the precipitation). The total diabatic heating rate is then determined by summing the latent and sensible heating rates.

The diabatic heating anomalies are shown in Figs. 3.2a and 3.3b for warm and cold SST anomalies, respectively. Strong near surface heating due to the warm SST anomaly decreases the convective stability of the air, increasing convection, precipitation and the diabatic heating rate over the SST anomaly region (Fig. 3.2a). Beyond the SST anomaly region, positive diabatic heating anomalies are limited to the tropics and parts of the subtropics. In much of the mid-latitudes, there is a decreased diabatic heating rate in response to the warm SST anomaly. The diabatic heating response to the cold SST anomaly is similar, but of opposite sign, to the response to the warm SST anomaly. There is a decrease in the diabatic heating rate over the cold SST anomaly, and the magnitude of the local response is less than it was with the warm SST anomaly. Similar to the warm SST case (though of opposite sign), negative (positive) diabatic heating anomalies extend downstream from the SST anomaly region in the subtropics (mid-latitudes). However, the anomalies become very weak and disorganized upstream of the SST forcing, indicating weak upstream diabatic heating in response to the cold SST anomaly. For this dissertation, we will refer to "upstream" and "downstream" in the context of west and east of the SST anomaly region, respectively. Unless otherwise noted, it does not imply a *direction* in which the anomalies propagate.

Increased diabatic heating (Fig. 3.2a) from the warm SST anomaly forces a negative geopotential height (pressure) anomaly in the lower troposphere over much of the SST anomaly region (Fig. 3.3a). Outside that region, the anomaly pattern is generally similar to that in Webster (1981), with waves propagating eastward and northward, and forming a wavenumber-one wave in the mid- and high-latitudes (30°-80°N). Meanwhile, the strong heating extends into the upper troposphere, forcing an upper-level high

pressure over most of the SST anomaly region from thermal expansion (Fig. 3.3c). Over the northwest part of the heating region, a low pressure anomaly can be found. The greatest height anomaly occurs slightly downstream of the greatest surface heating and is consistent with previous studies of similar heating anomalies (Webster 1981), largely due to the advection to the east of the upper-tropospheric heating by the upper tropospheric westerlies. Outside the heating source region, the geopotential anomalies in the upper troposphere also show a wavenumber-one wave propagating eastward and northward in the same latitude band as in the lower troposphere. These results are similar in many aspects to those found in previous studies using simplified models (e.g., Webster 1981, 1982; Hoskins and Karoly 1981). Two important differences between the upper and lower tropospheric geopotential height anomalies are that the upper troposphere anomalies are much weaker in the higher latitudes, compared to that in the lower troposphere, and that the larger anomalies in the upper troposphere are confined in the mid-latitude region between 30°-50°N.

The atmospheric circulation responses forced by the cold SST anomaly are quite different from that forced by the warm SST anomalies. In the lower troposphere, the major response to the cold SST anomalies is not near the region of the negative heating anomaly but quite some distance downstream and to the north of it (Fig. 3.3b). There is little response to the cold SST anomaly in the mid-latitudes, and the response is almost entirely confined to the high latitudes. The upstream response is also generally weaker than the response to the warm SST anomaly. In the upper troposphere, the circulation response is also much weaker in response to the cold SST anomaly and is confined between 30°-60°N latitudes (Figs. 3.3d).

Another way to look at the geopotential anomalies is from the perspective of mass transfer and that there are notable mass transfers between the subtropics and high latitudes in the lower troposphere. The geopotential height responses shown in Fig. 3.3 suggest that the mid- and high-latitude responses are generally barotropic north of 40°N and weakly baroclinic to the south. In response to the warm SST anomaly, there is a high-latitude barotropic high pressure upstream of the SST anomaly region that weakens with height and reduces the tropospheric mass (pressure) gradient upstream of the warm SST anomaly. Downstream of the SST anomaly, there is a barotropic low that also weakens with height. These anomalies extend out of the lower latitudes and show us that there is poleward mass propagation upstream of the warm SST anomaly and equatorward mass propagation downstream of the SST anomaly (Fig. 3.3a). In contrast, the anomalous mass fields in response to the cold SST anomaly indicate that there is a strong poleward transport of mass downstream of the SST anomaly (Fig. 3.3b). There is a broad equatorward mass transport further downstream, but it is generally weak in the areas immediately upstream of the cold SST anomaly. This strong asymmetry in the downstream and upstream lower tropospheric response to cold SST anomaly is not shown in the response to warm SST anomaly. This difference in symmetry of the lower troposphere response to the SST anomalies seems to suggest that the warm SST anomaly would have a greater ability to influence upstream low-level circulation, while both positive and negative SST anomalies are able to impact the downstream circulations. Furthermore, this pattern suggests that the anomalous waves are eastward propagating out of the SST anomaly region.

3.3 Direct Response to Continents

We next examine the direct effects of continental-scale land masses and how the resulting land-ocean contrast can modify the direct responses to North Atlantic SST anomalies. Any changes to the direct response to the SST anomalies would be due to interactions between circulations forced by the SST anomaly and the land surface represented by the idealized continents. The latter experiments will be referred to simply as the "land experiments" in the following discussions. To begin, we examine the direct response to the continental forcing using the zonally symmetric SST (Fig. 2.1b).

Figures 3.4a and 3.4b show the mean 850 and 200hPa winds and geopotential heights in the land experiment with the symmetrical SST. For clarity, we will sometimes refer to the changes forced by land on either the control or anomalous SST responses as the "land effect." The most noticeable effect of the lands in Figs. 3.4a and 3.4b is the zonal asymmetry in both the height and wind fields, forced by the asymmetry of the continental land masses. When compared to the aqua-planet results in Fig. 3.1, the asymmetry is not very strong, but there is still a definite impact of the continents on the circulation. This can be seen in the differences between the land and aqua-planet experiments with the control SST (Figs. 3.4c and 3.4d).

Figures 3.4c and 3.4d show the asymmetrical responses in geopotential heights and winds forced by the continental land masses. The land effect varies greatly as a function of the size and shape of the land mass. The large size and the idealized parallelogram shape of the Eurasian continent allows for the establishment of an anomalous continental-scale pressure system in the lower troposphere. Figure 3.5c shows that intense surface heating along the southern edge of the continent forces a

strong increase in temperature, especially to the west. This is due to the easterly trade winds being perturbed by the underlying continent. One impact of this heating is to increase the meridional temperature gradient over the southern edge of the continent, resulting in a northward expansion of the Hadley Cell over the southern part of Eurasia (Fig. 3.6). Intensification of the meridional circulation increases the poleward transport of mass and extends the subtropical high pressure northward.

In Fig. 3.4c, we see indications of the North Atlantic subtropical high pressure system (NASH). Figures 3.5b and 3.5d show the sea level pressure and better illustrate the NASH. The thermal difference between the ocean and surrounding continents is what forces the formation of the high pressure in the North Atlantic (Fig. 3.5a). While still slightly warmer than the same location in the aqua-planet simulation, the North Atlantic is slightly cooler than the surrounding continents, especially when compared to southern Eurasia. It is well known (e.g., Liu et al. 2004) that differential heating between land and ocean is a major forcing in the development of the NASH. In their study, they found that, if idealized sensible heating anomalies were imposed over the realistic locations of North America and Eurasia in an aqua-planet model, high pressure cells form over the North Atlantic and North Pacific. In this study, we allow for the surface temperature over land to change dynamically (Fig. 3.5c), and we obtain similar heating over the continents. The NASH in Fig. 3.5b is far less defined than in reality or the idealized experiments of Liu et al. (2004) and is likely due to several related factors. Sensible heating over the continents is far weaker in the current study than in Liu et al. (2004). Davis et al. (1997) also showed that the NASH is relatively weak in spring and does not fully intensify until early summer, likely as a result of a weaker land-ocean temperature contrast. Furthermore,

orography has also been shown to be an important forcing on the subtropical high pressure (Rodwell and Hoskins 2001) and is still absent in these land-only experiments. However, despite lacking these factors, the model is capable of forming a weaker, though still distinct, version of the subtropical high pressure system over the North Atlantic.

Over North America, a similar temperature pattern is found (Fig. 3.5c). However, the smaller portion of the continent in the subtropics limits the magnitude of the heating to a lesser amount, while the relatively small insolation in the mid-latitudes limits heating to north of 40°N over the continent. The heating over the southern part of the continent weakens the subtropical high pressure in the lower troposphere near the west coast of North America (Figs. 3.4a and 3.5d).

Comparisons of the circulations in the experiments with lands (Figs. 3.4a and 3.4b) to the aqua-planet case (Figs. 3.1a and 3.1b) suggest that the inclusion of land begins to establish some of the observed atmospheric patterns, although the land effects are still rather minor.

3.4 Responses to Warm and Cold SST Anomalies with Continents

We next examine how the continents can modify the atmospheric response to SST anomalies similar to the AMO. For this, we add a warm or cold SST anomaly in the North Atlantic Ocean to the land experiment. By comparing the results of the land experiments to the results from the aqua-planet simulations with the same SST anomalies, we can identify any modifications induced by land to the original SST forced atmospheric response.

The effects of the warm and cold North Atlantic SST anomalies on atmospheric circulation in presence of the continents are shown in Figs. 3.7a-d. We also include in Figs. 3.7e-h the differences between the continents and aqua-planet responses. These differences are determined by removing the response to the warm SST anomaly in the aqua-planet experiments from the response to the warm SST anomaly in the land experiments and are given as

$$\Delta Z_{mod} = \left(Z_{warm/cold} - Z_{control}\right)_{land} - \left(Z_{warm/cold} - Z_{control}\right)_{aqua} \qquad (3.1)$$

Using these differences, we can quantify how land alters the response to the SST anomaly. Another way to look at these differences is that they represent how land modifies the response to the SST anomalies. By understanding how the response to the warm SST anomaly can be modified by land, we can get an idea as to how variations in the land forcing might impact the observed AMO response. If the changes forced by land are small, the impact of any interannual variability in the land forcing would also likely be small. Similarly, if there are large changes forced by land, they could make the AMO forced response more variable from year-to-year and potentially change the time-mean response.

We first focus on the total effect of the warm SST anomaly on the circulation in presence of idealized, no-relief continents, and then highlight modifications forced by these continents. At 850 hPa, the response to the warm SST anomaly when land is present (Fig. 3.7a) is quite similar to the aqua-planet response to the warm SST anomaly (Fig. 3.3a). As in the aqua-planet simulations, the primary circulation responses to the warm SST anomaly in the lower troposphere are geopotential height anomalies that propagate northeastward out of the mid-latitudes. The anomalies propagate northward,

becoming “trapped” in the high-latitudes and extending toward the east. Specifically, a negative height anomaly extends northeastward from the SST anomaly region. Meanwhile, positive anomalies develop to the north and west of the SST anomaly region. The main differences between the land and aqua-planet experiments are that the magnitude of the anomalies in the land experiments is greater in the mid-latitudes and there are slight shifts in the locations of the anomaly centers. For example, the fairly uniform upstream ridge found in the aqua-planet simulation (Fig. 3.3a) is organized into two distinct centers in the land experiment, one over the North Pacific and the other near the northeastern corner of North America. The anomaly centered in the North Pacific is further to the west and the North American anomaly center is further to the east, and both are stronger than the aqua-planet anomaly (Figs. 3.7a vs. 3.3a). These changes leave a weaker positive anomaly over the northwestern corner of North America. Over the rest of North America, there is a southward extension in the positive geopotential heights, producing a broad region of higher geopotential over the continent in response to the warm SST anomaly. Downstream, the trough seen in the aqua-planet simulation is better organized and stronger in the land experiment. Instead of two distinct low pressure centers, there is just one that is centered over the Eurasian continent. In both the upstream and downstream directions, the direct responses to the SST anomaly in the mid-latitudes are replaced by an extension of the responses from the higher latitudes.

In the upper troposphere, the responses to the warm SST anomaly are generally weaker when land is included in the model (Figs. 3.7c vs. 3.3c). There are few notable changes in the pattern, but there are widespread decreases in the anomaly magnitudes. Comparison of the land effect (Fig. 3.7g) to the direct response to the warm SST anomaly

(Fig. 3.3c) reveals that the modification forced by land acts in opposition to the SST forcing.

The similarity of the lower tropospheric responses to the warm SST anomalies between the model runs with and without continents (Figs. 3.7a and 3.3a) suggest the land effect is relatively small (Fig. 3.7e). Some subtle and interesting differences between the aqua-planet and land experiments are seen, however, when forced by the warm SST anomaly. For example, the land effect increases (decreases) the geopotential heights over most of North America (Eurasia). This pattern bears interesting resemblance to both the direct land forcing and direct SST forcing, though of opposite polarity (Figs. 3.4c and 3.3a vs. 3.7e). There are interesting implications about these dissimilarities. Most notably, they indicate that the direct responses to land and the warm SST anomaly are non-commutative and exhibit additive nonlinearity when they interact. When the land forced response (Fig. 3.4c) is added to the SST forced response (i.e., aqua-planet; Fig. 3.3a), rather than an enhancement the SST response as one would expect from the similarities between the two, the SST forced response is slightly weakened over the continents (Fig. 3.7e). This is especially apparent over Eurasia. The weakening of the response suggests a feedback mechanism from the land that acts to weaken the direct SST response, despite the direct land forcing being favorable for the opposite.

To understand this mechanism, we can look at the anomalous surface temperatures forced by the warm SST anomaly in the presence of land (Fig. 3.8a) and the modifications caused by the continents (Fig. 3.8b). Downstream of the warm SST anomaly, there is strong advection of heat from the North Atlantic into the southern half of Eurasia. Near 60°E longitude, some of the heat is advected from the subtropics into

the mid-latitudes. This heat advection downstream of the North Atlantic only occurs when land is present (Fig. 3.8b), but it is not a direct response to the continent (as the direct effect of the continent is removed in Fig. 3.8b). Rather, it is a modification by land on the warm SST forced response. The modifications by land force warmer surface temperatures of about 1°C over most of Eurasia, and thermal expansion reduces the lower tropospheric pressure and geopotential heights (Fig. 3.7e). When the warm air is advected over the continent, it heats the underlying surface. Once heated, there is an increase in sensible heat flux from the surface that enhances the atmospheric heating in the lower troposphere. As a result of this feedback, the model equilibrates with warmer temperatures and lower heights in the lower troposphere over most of Eurasia when land is present. This is consistent with the observational study of Sutton and Hodson (2005), who found that temperatures over Eastern Europe are significantly warmer in boreal summer during the warm phase of the AMO than in the cold phase. Because the current study is run to equilibrium, the heating shown here may help to explain the source of the anomalous heating over Europe in summer. Therefore, even though the direct responses to both the land and warm SST anomaly should act to increase the heights over Eurasia, the additional heating over Eurasia forces a weakening of the SST forced circulation response over the continent.

An exception to this is over the northeastern corner of Eurasia, where the modification by land on the warm SST response is positive (Fig. 3.7e). A different process is likely at work here. When the warm air is advected over the relatively cool ocean, the near-surface layer cools more quickly than the overlying layers. The cooling of the lower troposphere and the relatively warmer middle and upper troposphere produce

a barotropic high pressure (Figs. 3.7e and 3.3g). It is this anomalous high pressure that acts to extend the upstream high pressure farther to the west (Figs. 3.7a vs. 3.3a).

Over North America, the heating (or cooling) effect is much smaller and limited to the far northern or southern reaches of the continent (Fig. 3.8a), most likely due to the smaller size of the continent. The high-latitude negative geopotential heights in Fig. 3.7e are likely forced in part by the warmer surface temperatures along the northern coasts of the continent. However, the causes behind the increased geopotential heights over much of North America are less clear, especially considering there is weak heating over North America. One possibility is that it is simply a remote response to the forcing over Eurasia. In the mid-latitudes, the negative anomaly over Eurasia and the positive anomaly over North America form a wavenumber-one wave (Fig. 3.7e). This is similar to the wave forced by diabatic heating in Ting (1994). In this study, heating over Eurasia is capable of forcing a positive lower tropospheric streamfunction anomaly over North America and the North Atlantic. Additionally, Ting (1994) found that a negative anomaly forced by North American diabatic heating is masked by the positive anomaly forced remotely by Eurasia. Therefore, it is possible that Eurasia remotely forces the geopotential height increase over North America during the warm phase of the AMO. The wave pattern weakly extends barotropically through the troposphere.

It is also possible to examine these differences from another perspective. For this, we can rewrite (3.1) as

$$\Delta Z_{mod} = \left(Z_{land} - Z_{aqua}\right)_{warm/cold} - \left(Z_{land} - Z_{aqua}\right)_{control} \qquad (3.2)$$

This equation shows how the direct land effect is modified by the warm SST anomaly. Because (3.2) is mathematically equivalent to (3.1), Figs. 3.7e-h, 3.8b and 3.8d are also

valid with (3.2). However, as mentioned earlier, this can be compared to the direct response to land (Fig. 3.4c) to see how the features forced by the land-ocean contrast are modified by the warm SST anomaly. It is apparent when comparing Figs. 3.4c to 3.7e that the responses due to the presence of land are weakened over both continents, but the high pressure over the North Atlantic is largely unchanged. The heating over Eurasia in the mid-latitudes (Fig. 3.8b) acts to weaken the subtropical temperature gradient, thereby weakening the Hadley circulation and decreasing the mass transport northward and reducing the continental high pressure.

Land modifies the response to the cold SST anomaly in a far different way than it modifies the response to the warm SST anomaly. When comparing the lower tropospheric responses to the cold SST anomaly and land (Figs. 3.3b and 3.4c, respectively), it becomes apparent that the patterns are in almost complete opposition to each other. However, when these opposite effects are produced simultaneously, they do not cancel out. In Fig. 3.7f, we find that the modifications by land to the circulation forced by the cold SST anomalies are strongest in the mid- and high-latitudes in North America and Eurasia. A pair of anomaly dipoles develop from the effects of the continents, with a positive (negative) anomaly center over the northeastern (northwestern) corner of each continent. The dipoles extend barotropically through the troposphere, but the magnitudes of these dipoles are more significant in the lower troposphere (Figs. 3.7f vs. 3.7h). The effects are also weak in the low-latitudes south of the 30ºN.

These dipoles of geopotential height anomalies completely redefine the circulation anomaly patterns in response to the cold SST anomaly in the lower and upper

troposphere (Figs. 3.7b and 3.7d) from that forced by the cold North Atlantic SST anomaly alone (Figs. 3.3b and 3.3d). A major effect of these dipoles is that they help form deformation fields over Eurasia and North America. For the most part, the anomalous deformations from the land effect serve to weaken the mid- and high-latitude responses to the cold SST anomaly. This is particularly evident over Eurasia, where the direct response to the cold SST anomaly is almost completely eliminated and only weak anomalies remain. The inclusion of land forces a positive anomaly over the northeastern corner of North America and a strong negative anomaly over the northwestern corner of the continent in the lower troposphere. In the upper troposphere, the polarity remains the same, but the negative anomaly weakens and the positive anomaly strengthens. Because of the small size of North America in the subtropics, the deformation field is primarily determined by the strong dipole in geopotential height anomalies along the northern coasts of the continent. However, there are weak anomalies in the subtropics that support the positioning of a deformation field in the center of the continent and southerly anomalies in wind (Fig. 3.7b).

The changes of the surface temperature response to the cold SST anomaly (Fig. 3.8d) do not readily explain the changes in the circulations forced by the inclusion of land. Both continents exhibit similar circulation dipoles along their northern coasts, but have very different temperature anomalies, warm over North America and cold over Eurasia. Further research is needed to better understand the causes behind the dipoles.

Regardless of the source of these dipoles, they act to weaken the downstream response and greatly enhance the upstream response to the SST anomaly in the North Atlantic. This produces features that resemble those from other studies. For example,

the relatively strong positive geopotential height anomalies over northeastern North America and northwestern Eurasia (Fig.3.7b) are reminiscent of anomalies described in the observational analysis of Hu and Feng (2008) and the modeling study of Hu et al. (2011). While there is some variation in the details, Hu and Feng (2008) displayed a similar high pressure anomaly across the North Atlantic around 60°N during the cold phase of the AMO. Likewise, Hu et al. (2011) show a high pressure center during the cold phase in the western North Atlantic that is slightly to the southeast of the one in this study. Consistent results such as these suggest that the modifications of North American circulations by land can be a major influence during the cold phase of the AMO. Furthermore, we have shown that the strong modifying effect by land on the circulation is important in transforming the otherwise quite weak circulation anomalies over North America (Fig. 3.3b) into a relatively strong and coherent pattern.

There is a potential for the land-modified response to the cold SST anomaly to have teleconnections with other remote forcings. Examination of the geopotential height anomalies in response to the cold SST anomaly indicates that the anomalies show some similarity to the positive phase of the Pacific-North American pattern (PNA; Wallace and Gutzler 1981). The upper tropospheric circulation anomalies (Fig. 3.7d) are negative in the northwestern and southeastern part of North America and positive in between from the northeast through the southwest. These anomalies and those in the central Pacific depict a wave train from the tropical Pacific to the southeastern part of North America. Meanwhile, the negative anomaly in northwest North America, a feature consistent with the Aleutian Low, is the only strong anomaly in the lower troposphere (Fig. 3.7b). This pattern in the upper and lower troposphere is consistent with that shown in Fig. 5 of

Wallace and Gutzler (1981). These similarities suggest that the cold SST anomalies in the North Atlantic (i.e., the cold phase of the AMO) could potentially force circulation anomalies that interact with the anomalies developing the positive phase of the PNA. With warm SST anomalies in the North Atlantic Ocean, the land effect of North America is shown to enhance the positive height anomalies in northeastern North America and shows little influence on the geopotential height in the northwestern corner of the continent. Thus, warm SST anomalies in the North Atlantic would be unlikely to enhance the negative phase of the PNA.

3.5 Direct Response to Continents and Orography

To examine how significant topographic features on continents further modify the atmospheric circulations forced by the SST anomalies in the North Atlantic Ocean, we now add idealized representations of the Rocky Mountains, the Alps and the Tibetan Plateau to the idealized North American and Eurasian continents. As we did when land was added to the model, we will refer to the changes forced by orography on the responses to the control and anomalous SSTs as the "orography effect." The impact of the orography on the atmospheric circulation is immediately apparent from comparisons between the model runs with land and orography and those with land, but no orography (Figs. 3.9 vs. 3.4). We first notice that the geopotential height differences between land and orography and land without orography cases (Figs. 3.9c and 3.9d) are about three times as large as the differences between the aqua-planet and land experiments (Figs. 3.4c and 3.4d). These large differences clearly indicate a strong orographic effect on atmospheric circulation.

The effect of orography is shown primarily through the forcing of stationary eddies in the troposphere that distort the zonal flow over and near each orographic feature. In North America, the effect of the Rocky Mountains is shown by the positive geopotential anomalies along the northern edge of the Rockies that extend into the higher latitudes (Fig. 3.9c). Negative geopotential anomalies develop along the southern edge of the Rockies and extend into the subtropics. In the lee of the Rocky Mountains, the lower geopotential and north-south orientation of the terrain produce southerly flows in the lower troposphere from over the ocean in the south to central North America. These anomalies are similar to that described in the idealized experiments of Brayshaw et al. (2009). Similar geopotential height anomaly patterns are shown around the Alps and the Tibetan Plateau, though the magnitudes of the anomalies differ. The stationary eddies forced by the Alps are barely noticeable in Fig. 3.9c, whereas the massive and oval shaped Tibetan Plateau forces a strong distortion of the flow around it (Figs. 3.9c and 3.9d). In the lower troposphere, the Plateau extends above the 850 hPa level, diverting the westerly flow to the south and north around the Tibetan Plateau. This diversion of the westerly flow forces strong anomalous meridional (zonal) flow along the western (northern) and eastern (southern) flanks of the Plateau.

Another effect of the orography is the overall increase of the geopotential north of 50ºN, particularly in the lower troposphere. These anomalies in geopotential height suggest a warmer atmosphere in the high latitudes imposed by orography and is consistent with the known effect of orography on northward eddy heat transports (e.g., Peixoto and Oort 1992). Details of these eddy heat and momentum transport processes and their resulting effects are a potential topic for future work. However, it is important

to note that these enhanced eddy processes and poleward heat transports by the orography increase the mass and temperature, and therefore the geopotential height in the higher latitudes, and reduce the mass and geopotential in the lower latitudes. This mass and heat transport is evident in the sea level pressures, where the high-latitude pressures are greater by about 8-10 hPa (Fig. 3.10d). These mass adjustments forced by orography act to reduce the meridional pressure gradient and the zonal winds across the mid-latitudes (Figs. 3.9c and 3.9d).

Decreases of the zonal wind across the entire mid-latitudes extend far beyond the orographic features themselves (Brayshaw et al. 2009). This means that in addition to forcing the local eddies, the orography forces easterly flow anomalies around the entire mid-latitudes. This is consistent with the impact of frictional and mountain torques on decreasing the angular momentum in the mid-latitudes (e.g., White 1949; Newton 1971). Furthermore, the consistent easterly wind anomalies in the mid-latitudes in the lower and upper troposphere indicate that orography weakens the mid-latitude westerlies throughout the entire troposphere (Figs. 3.9c and 3.9d).

The combined effects of the orography and continental forcings are shown in Figs. 3.9a and 3.9b for the lower and upper troposphere, respectively. In the lower troposphere, the negative anomalies forced along the southern flank of the orography act to decrease the subtropical high pressure along the southern edge of the Rockies and Tibetan Plateau. This further weakens the subtropical high pressure over North America and the North Pacific when compared to the land experiment (Fig. 3.4a). Over Eurasia, the location of the Tibetan Plateau and resultant negative anomalies strongly alter and weaken the subtropical high pressure. As a result of the weakening of subtropical high

pressures over the continents, the NASH is more clearly defined in the North Atlantic and can be seen when examining the sea level pressure response in the experiment with orography (Fig. 3.10b). The features shown in Fig. 3.10b indicate that the simulated NASH much more closely resembles the observed NASH (Hu et al. 2011). This helps produce a stronger southerly component to the wind over North America (Fig. 3.9a). Closer examination of Fig. 3.9a shows that the southerly flow is weaker and displaced eastward in longitude compared to observations. The highly idealized representation of the North American continent and its orography are likely major contributors to these deviations from observations. Even with these differences, the low-level southerly flows over eastern North America and the NASH are better defined with the idealized orography than without.

The response to land and orography in the upper troposphere (Fig. 3.9d) is similar to that in the lower troposphere. As indicated by Fig. 3.9d, the nearly uniform positive geopotential anomalies in the high latitudes and negative height anomalies in the low latitudes indicate poleward mass transport by circulation anomalies induced by orography. These adjustments in mass and heat forced by orography result in increased geopotential heights in the high-latitudes and decreased heights in low-latitudes. In addition, there are reduced zonal westerly winds in the mid-latitude as well as decreased vertical shear of the zonal winds, thus reducing baroclinicity. This will be revisited in the discussions about precipitation in Chapter 4.

3.6 Responses to Warm and Cold SST Anomalies with Orography

We now examine the roles of orography in modifying the circulation response to the North Atlantic SST anomalies. Similar to the previous section, we calculate the geopotential height differences between the land without orography and the land with orography experiments with positive or negative SST anomalies in the North Atlantic Ocean (Fig. 3.11). We use a modified version of equation (3.1) and by taking these differences, we can evaluate how orography modifies the circulation response to the warm or cold SST anomalies.

The results shown in Fig. 3.11a suggest that the orographic effect of the lower tropospheric response to the warm SST anomalies is still relatively small. There are few major differences in the circulation responses between the experiments with and without orography (Figs. 3.11a vs. 3.7a). Downstream of the SST anomaly in the North Atlantic, the response to the warm SST anomalies is still dominated by a negative height anomaly (Fig. 3.11a). However, the center of the anomaly is shifted toward the northwestern corner of Eurasia. This may possibly be an effect of the Alps interrupting the anomalous flow and diverting the anomalies. Upstream of the warm SST anomaly, the positive anomalies in geopotential still occur, but they are also shifted toward the north with orography. These anomalies suggest that orography acts to deflect the circulation responses out of the mid-latitudes toward the high-latitudes, leaving the mid-latitudes under a strongly modified regime.

Similar to the land effect, the orographic effect generally extends barotropically through the troposphere (Fig. 3.11g). If we compare Figs. 3.11c to 3.7c, we see that there is an intensification of the mid-latitude circulation response in the upper troposphere. In

the high-latitudes, the responses to the warm SST anomaly are somewhat weaker and shifted westward from their positions in the case without orography, and this tends to center most of the high-latitude response over the North Pacific and Atlantic basins.

The modifications by orography on the surface temperatures forced by the warm SST anomaly (Fig. 3.12b) are not nearly as extensive as the modifications forced by land alone (Fig. 3.8b). There are a few exceptions, however. Over North America, the high-latitudes experience cooler temperatures, reversing the land-only warming, and producing effectively neutral temperature anomalies when all factors are included (Fig. 3.12a). Recall that most of North America had warmer temperatures with land present, but that the remote forcing from Eurasia overwhelmed the local circulation response (Figs. 3.7a and 3.8a). The land and orographic effect over North America are now complimentary in the mid-latitudes and, as a result, the effect of the remote Eurasian forcing is diminished. Over Eurasia, the strongest temperature anomalies are located in the northwest and further contribute to the overall warming of the continent in response to warm North Atlantic SST. Interestingly, there is only a weak temperature response around the Tibetan Plateau. This suggests the Tibetan Plateau does little to modify the lower tropospheric temperatures in response to the warm SST anomaly. This is not to be confused with the direct response to the plateau, which is extensive.

During the warm phase of the AMO, the northward mass transport is enhanced near North America but reduced over Eurasia, producing relative high and low pressures, respectively (Fig. 3.11a). This produces a zonal mass (pressure) gradient across the high-latitude North Atlantic and induces a northerly component to the westerlies, bringing colder polar air from the north. One consequence of this anomalous flow is that it

reduces the temperatures in northern Europe (Fig. 3.12b) and bears similarity to the springtime results of Sutton and Dong (2012) and Feng and Hu (2008). In the observational study of Sutton and Dong (2012), they found that the European springtime temperatures differences between the warm and cold phases of the AMO are not as strong as they are in summer, particularly in eastern and northern Europe. They also show relatively similar pressure anomalies near Europe (their Fig. 4) as we found in the current study (Fig. 3.11a). These similarities, despite the large differences in study design, suggest that warming over eastern and northern Europe in response to warm SSTs may be offset during spring by anomalous northerlies.

With the cold SST anomalies in the North Atlantic Ocean, the modification of the circulation by orography once again differs from the land-only response (i.e., Figs. 3.11b vs. 3.7b). Downstream of the North Atlantic, there are relatively minor changes, with most of Eurasia having slightly greater geopotential heights in response to the cold SST anomaly (Fig. 3.11f). As a result, the weak deformation field over Eurasia forced by the land effect (Fig. 3.7b) no longer exists and is replaced by a better defined positive anomaly that extends out from the North Atlantic. On the other hand, the upstream response to the cold SST anomaly is strongly modified by orography, which forces another strong dipole in the high-latitudes. This dipole is of opposite polarity and shifted slightly upstream from the dipole produced by the land effect and results in a single negative geopotential anomaly in the high-latitudes near North America (Fig. 3.11b). The negative anomalies extend weakly into the mid-latitudes and cover much of the continent. In the upper troposphere, strong orography-forced changes are largely limited to the Western Hemisphere (Fig. 3.11h) and closely resemble the lower troposphere

response, indicating that the changes are barotropic. The positive anomaly over much of North America (Fig. 3.11d) and the negative anomaly to the north indicate an anomalous frontal zone across the northern part of continent that bears some similarity to a frontal zone during boreal summer in the realistic simulations of Hu et al. (2011).

The modifications of the temperature due to orography (Fig. 3.12d) and the response forced by the cold SST anomalies in the presence of land and orography (Fig. 3.12c) bear some interesting resemblance to the paleoclimate results of Feng and Hu (2008). In their study, they found good correlation between cool North Atlantic SSTs representative of the cold phase of the AMO and a cooler Tibetan Plateau. Examination of their Fig. 2a indicates that this correlation occurs during spring as well as summer, between 80°-120°E longitude, and 20°-40°N latitude. This is consistent with the orographic modification of the response to the cold SST anomaly in this study (Fig. 3.12d) and suggests that the connection between the Tibetan Plateau temperature and North Atlantic SST is a basic response and that even with a highly idealized surface boundary and no other forcings, it is still evident. Furthermore, the connection between Tibetan Plateau and North Atlantic temperatures (Fig. 3.12b) is much weaker during the warm phase in both the current study and Feng and Hu (2008). Therefore, the current study reaffirms the paleoclimate results of Feng and Hu (2008) and suggests that the cold phase of the AMO can have an important impact on monsoonal patterns in southern and southeastern Asia.

Interestingly, the changes in circulation forced by orography on the responses to both warm and cold SST anomalies are quite similar (Figs. 3.11e-h). In both cases, the strongest and most organized changes to the circulation tend to occur upstream of the

North Atlantic. This is especially true for the cold phase of the AMO, where the response over Eurasia is far weaker than the response near North America. One reason for this may be the similar temperature responses to the warm and cold SST anomalies when land is present (Figs. 3.12b and 3.12d). When the orography-modified circulations are added to the direct SST forced response (Figs. 3.11a-d), the upstream responses are generally stronger than the downstream responses, with the exception of the areas immediately downstream. From this, we can conclude that in the presence of the major permanent forcings (land and orography), the strongest responses to the warm and cold phases of the AMO are immediately downstream of the North Atlantic and upstream over North America. There are exceptions to this, such as the impact on the South Asian monsoon, but the stronger responses tend to be upstream.

3.7 Chapter Summary and Major Findings

In this chapter, we examined the roles and interactions between SST anomalies in the North Atlantic (similar to the AMO), continental land masses and orography using the CESM1.0.5 with idealized surface boundaries (see Chapter 2 for details). These simulations have shown that the modifications by land and orography on the direct response to the SST anomalies vary depending on the polarity of the SST anomaly and that the interactions between the forcings can be quite complex.

The response to the aqua-planet surface boundary (Fig. 3.1) is simple and zonally symmetric, with the expected circulations forced by the three-cell meridional circulation (Peixoto and Oort 1992). When continents are added to the model, asymmetry is introduced in the circulation (Fig. 3.4) and several notable features are seen (Fig. 3.4c).

The first is the initial formation of the North Atlantic subtropical high pressure (NASH) in response to the land-ocean temperature contrast. The second is a shift in mass towards the center of Eurasia from an increase in the Hadley cell due to a strengthening of the meridional temperature gradient over the continent. A third is the development of a thermal low over North America.

Overall, these changes are small compared to how orography alters the atmospheric circulation. With orography, there is a strong transport of mass poleward, particularly near the Rocky Mountains and the Tibetan Plateau (Fig. 3.9), which weakens the mid-latitude westerlies globally. Additionally, the stronger mass transports near the orography act to further isolate the NASH, and it becomes strong enough to produce southerly winds along its west flank near North America (Figs. 3.9c and 3.10b).

In the aqua-planet experiment with warm SST forcing, it was found that strong diabatic heating in the North Atlantic (i.e., the latitude and longitudes of the North Atlantic), forces low geopotential heights in the lower troposphere that extend toward the northeast. Downstream of the SST anomaly region, positive geopotential height anomalies extend from the subtropics toward the northeast (Fig. 3.3a). These two patterns form a wavenumber-one wave in the mid- and high-latitudes that extends barotropically into the upper troposphere (Fig. 3.3c). Near the subtropics, the tropospheric response is more baroclinic. The upstream response is of comparable magnitude to the downstream response.

When the continents were added to the model, the interaction between the warm SST anomaly and the land forces an anomalous deformation field in addition to the direct response to the SST anomaly (Fig. 3.7e). The effect of the deformation is relatively small

compared to the strong direct response to the warm SST in the North Atlantic (Fig. 3.3a). However, it generally enhances the direct response to the SST in the high-latitudes and expands the high-latitude response into the mid-latitudes (i.e., high pressure over North America and low pressure over Eurasia), reversing the direct response to the warm SST anomaly (Fig. 3.7a). The Eurasian continent amplifies the temperature anomalies forced by the warm SST anomaly (Fig. 3.8b). This in turn, forces a global wavenumber-one response in the mid-latitudes. When orography is included, the mid-latitude response weakens, effectively shifting the strongest of the responses to the north. In general, the land-only case acts to expand the high-latitude response into the mid-latitudes, and the addition of orography weakens or reverses that expansion. However, the pattern remains relatively consistent in the high-latitudes, regardless of these changes in the underlying surface boundary.

This is not the case for the cold SST anomaly. The pattern of the circulation anomalies is quite susceptible to changes in the surface boundary, particularly upstream of the North Atlantic. In the aqua-planet simulation, most of the response is confined to the high-latitudes and there are only small changes in the mid-latitudes (Figs. 3.3b and 3.3d). The anomalies form a wavenumber-one wave of opposite polarity compared to the warm SST response, though the wave is weaker and more meridionally spread out.

The cold SST anomaly interacts with land to produce a pair of dipoles in the northern parts of North America and Eurasia (Fig. 3.7f) in addition to the direct response to the SST anomaly. This greatly weakens the response to the cold SST anomaly, particularly in the high-latitudes. When orography is added to the model, the pattern

changes once more, but not as drastically as it did with the addition of the continents (Fig. 3.11b vs. 3.7b).

In summary, the response to a warm North Atlantic Ocean is generally strong, regardless of the surface boundary configuration. When lands and orography are added in the model, the response to the warm SST anomaly in the high-latitudes remains relatively constant, but the circulation response in the mid-latitudes exhibits variability depending on the surface boundary. In contrast, the response to the cold SST anomalies is highly dependent on the land surface configuration and can be seen clearly in the dramatic difference between the responses to the cold SST anomaly with the aqua-planet and land surfaces and the weaker, though still notable, change when orography is added. The modifications of the response also tend to be strongest upstream of the SST forcing. For both warm and cold SST anomalies, the orographic effects tend to be opposite of the land effect, and these effects interact to produce the complex circulation anomalies presented in this chapter. Clearly, the land and orographic forcings are quite important in producing the observed circulation patterns.

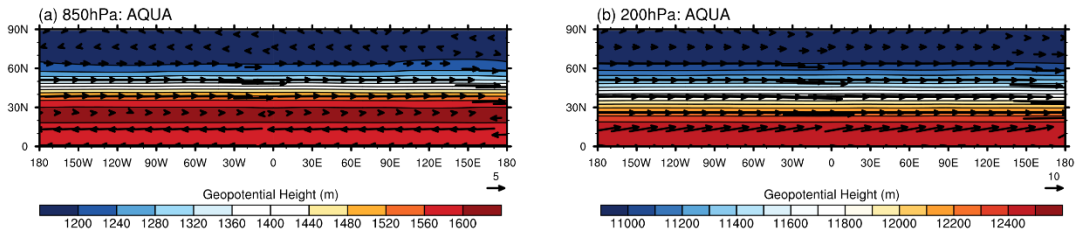

Figure 3.1: Mean geopotential heights and winds for the control SST in the aqua-planet experiment at (a) 200 hPa and (b) 850 hPa. Units are in meters (heights) and m s^{-1} (winds). Contour intervals and reference vectors are (a) 40 m, 5 m s^{-1} and (b) 100 m, 10 m s^{-1}.

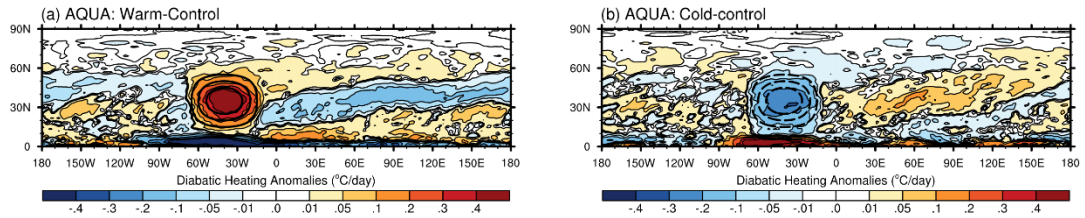

Figure 3.2: Anomalies in whole column diabatic heating (sensible + latent heat release) for the (a) warm and (b) cold SST anomalies. Units are in °C day^{-1}. SST anomalies are shown by the concentric circles. Concentric circles are the SST anomalies and are the same as Fig. 2.1, with solid (dashed) lines indicating a positive (negative) anomaly.

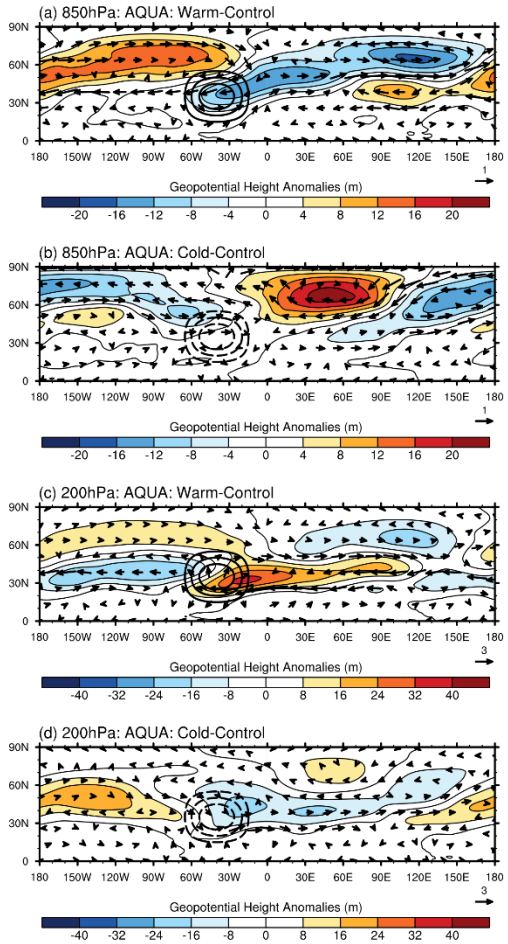

Figure 3.3: Anomalies of zonal perturbations of geopotential height and winds at (a,b) 850 hPa and (c,d) 200 hPa in response to the (a,c) warm and (b,d) cold SST anomalies in the latitudes of the North Atlantic Ocean. Units for geopotential height are meters and winds are m s^{-1}. Contour intervals and reference vectors are (a,b) 4 m, 1 m s^{-1} and (c,d) 8 m, 3 m s^{-1}. Concentric circles are the SST anomalies and are the same as Fig. 2.1, with solid (dashed) lines indicating a positive (negative) anomaly.

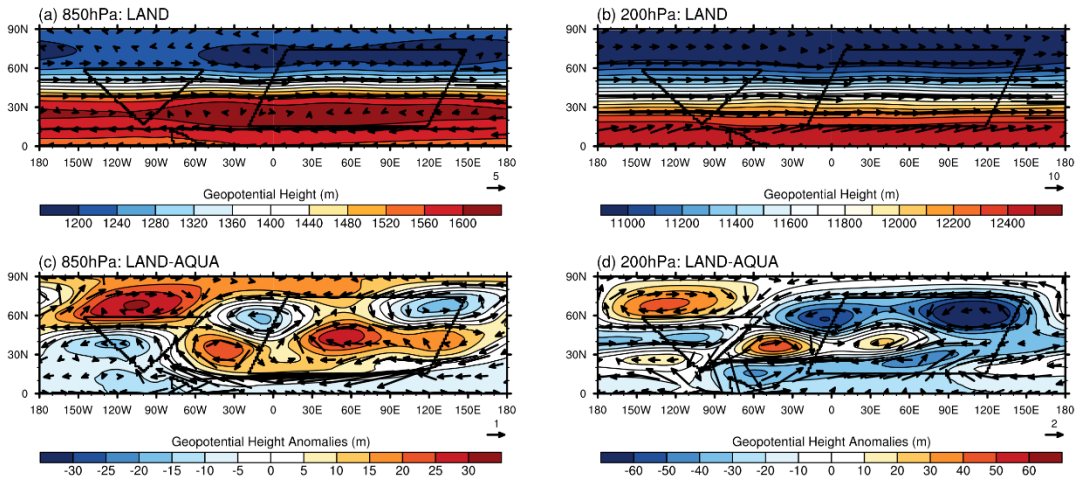

Figure 3.4: (a,b) are the same as Fig. 3.1, except for the land experiment. (c,d) are the differences between the land experiment and the aqua-planet experiment at 850 hPa and 200 hPa, respectively. Contour intervals and reference vectors are (a) 40 m, 5 m s^{-1}, (b) 100 m, 10 m s^{-1}, (c) 5 m, 1 m s^{-1} and (d) 10 m, 2 m s^{-1}.

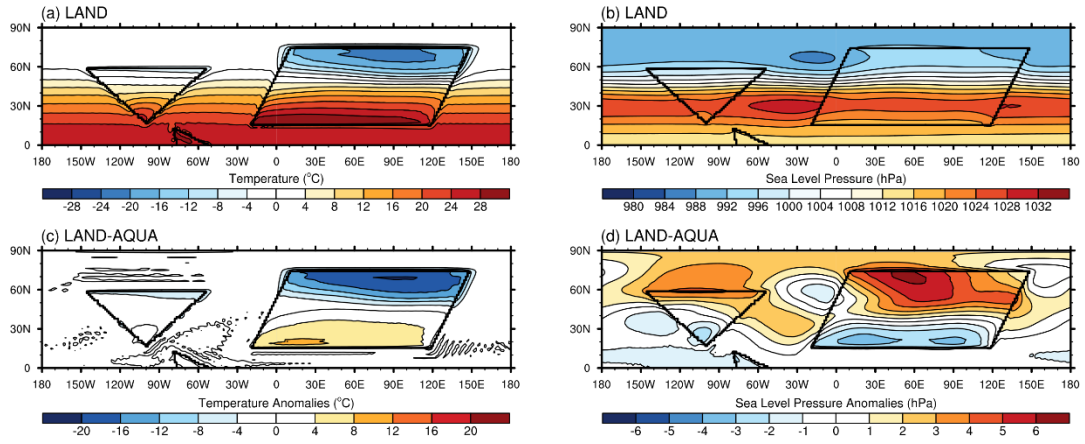

Figure 3.5: (a) surface temperatures in the land experiment with the control SST and (c) difference from the aqua-planet experiment. (b,d) are the same, but for sea level pressure. Contour intervals are (a,c) 4°C, (b) 4 hPa and (d) 1 hPa.

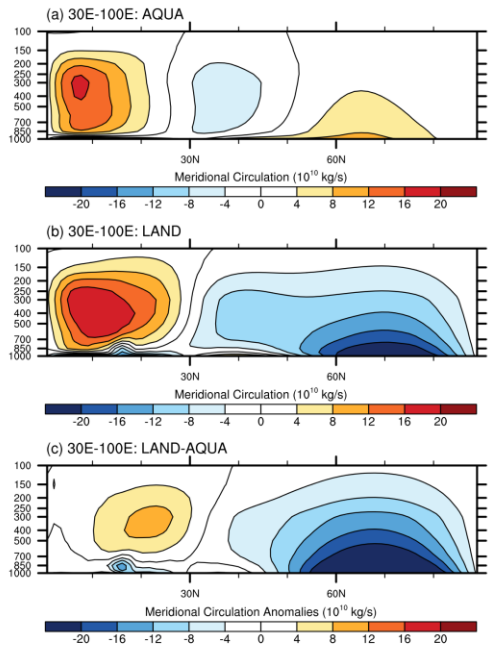

Figure 3.6: Meridional cross-sections (pressure and latitude) of the zonally averaged meridional circulation between 30°-100°E longitude for the (a) aqua-planet and (b) land experiments. (c) is the difference between the land and aqua-planet experiments. Contour interval is 4×10^{10} kg s^{-1}.

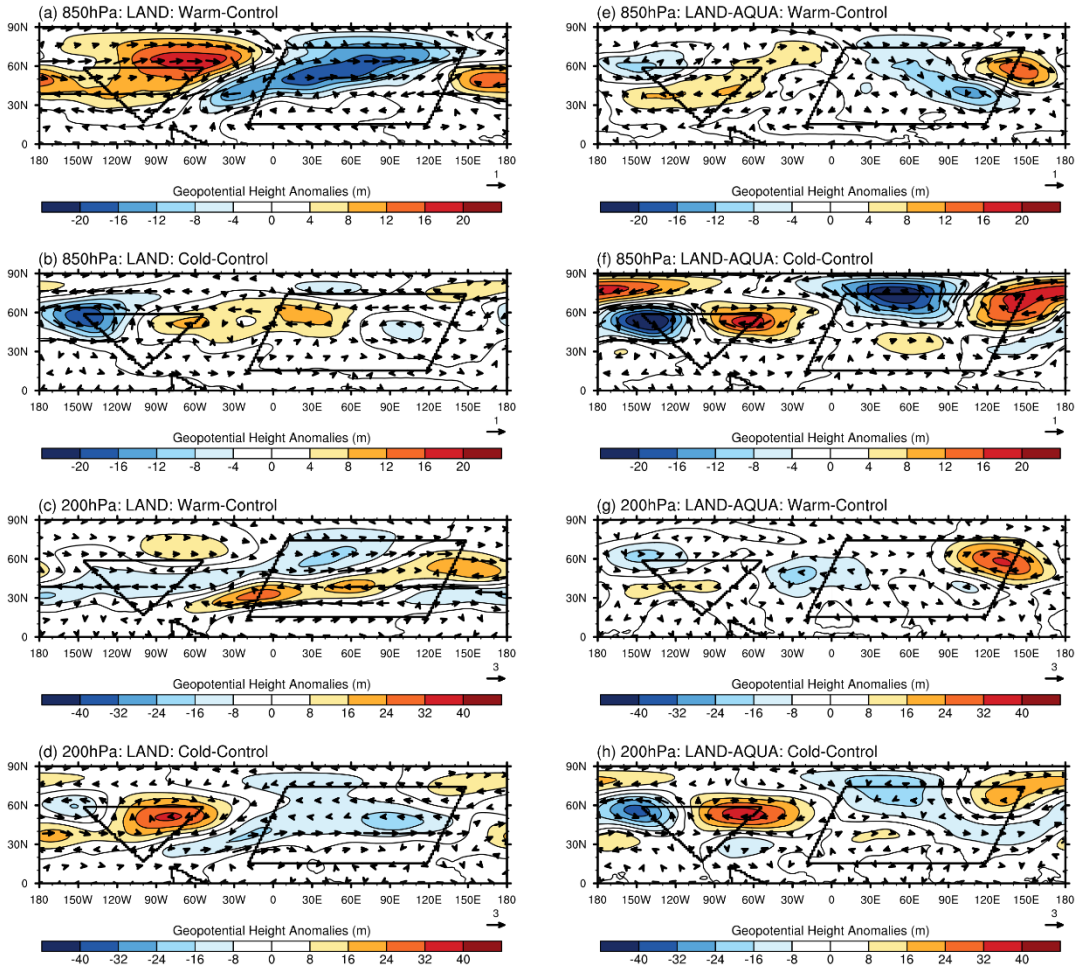

Figure 3.7: (a-d) are the same as Fig. 3.3, except for the land experiments and (e-h) are the differences between the land experiments and the aqua-planet experiments. Contour interval and reference vectors are (a,b,e,f) 4 m, 1 m s^{-1} and (c,d,g,h) 10 m, 3 m s^{-1}.

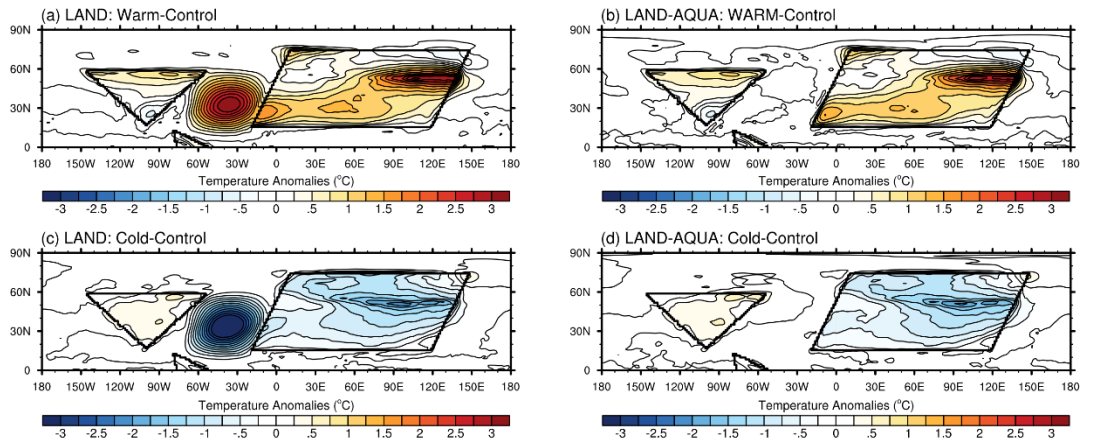

Figure 3.8: Surface temperature responses to the (a) warm and (c) cold SST anomalies in the presence of land and (b,d) are the differences between the land experiments and the aqua-planet experiments for the warm and cold SST anomalies, respectively. Units are in degree Celsius (°C) and contour interval is 0.25°C.

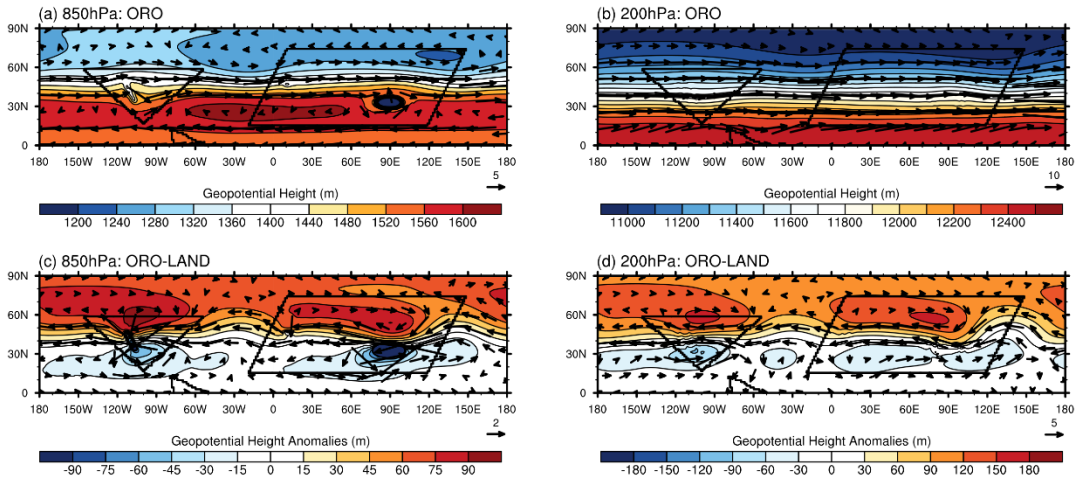

Figure 3.9: Same as Fig. 3.4, but for the orography experiment. (a,b) are the same as Fig. 3.4a and 3.4b, except for the orography experiment. The differences in (c,d) are between the orography experiment and land experiment. Contour interval and reference vectors are (a) 40 m, 5 m s^{-1}, (b) 100 m, 10 m s^{-1}, (c) 15 m, 2 m s^{-1} and (d) 30 m, 5 m s^{-1}. Note the increase of the contour intervals and reference vectors in (c,d) from Fig. 3.4.

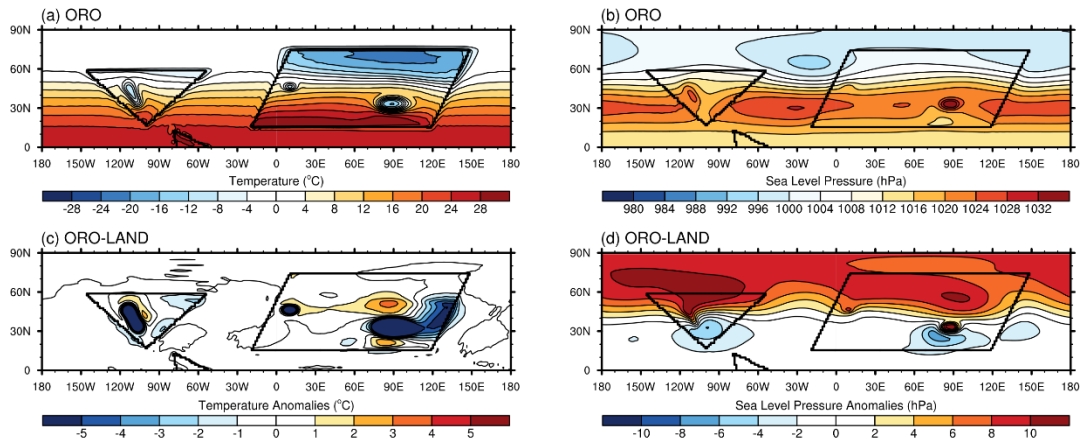

Figure 3.10: Same as Fig. 3.5, but for the orography experiment. (a,b) are the same as Fig. 3.5a and 3.5b, except for the orography experiment. The differences in (c,d) are between the orography experiment and land experiment. Contour intervals are (a) 4°C, (b) 4 hPa, (c) 1°C and (d) 2 hPa. As with Fig. 3.9, note change in scale from Fig. 3.5.

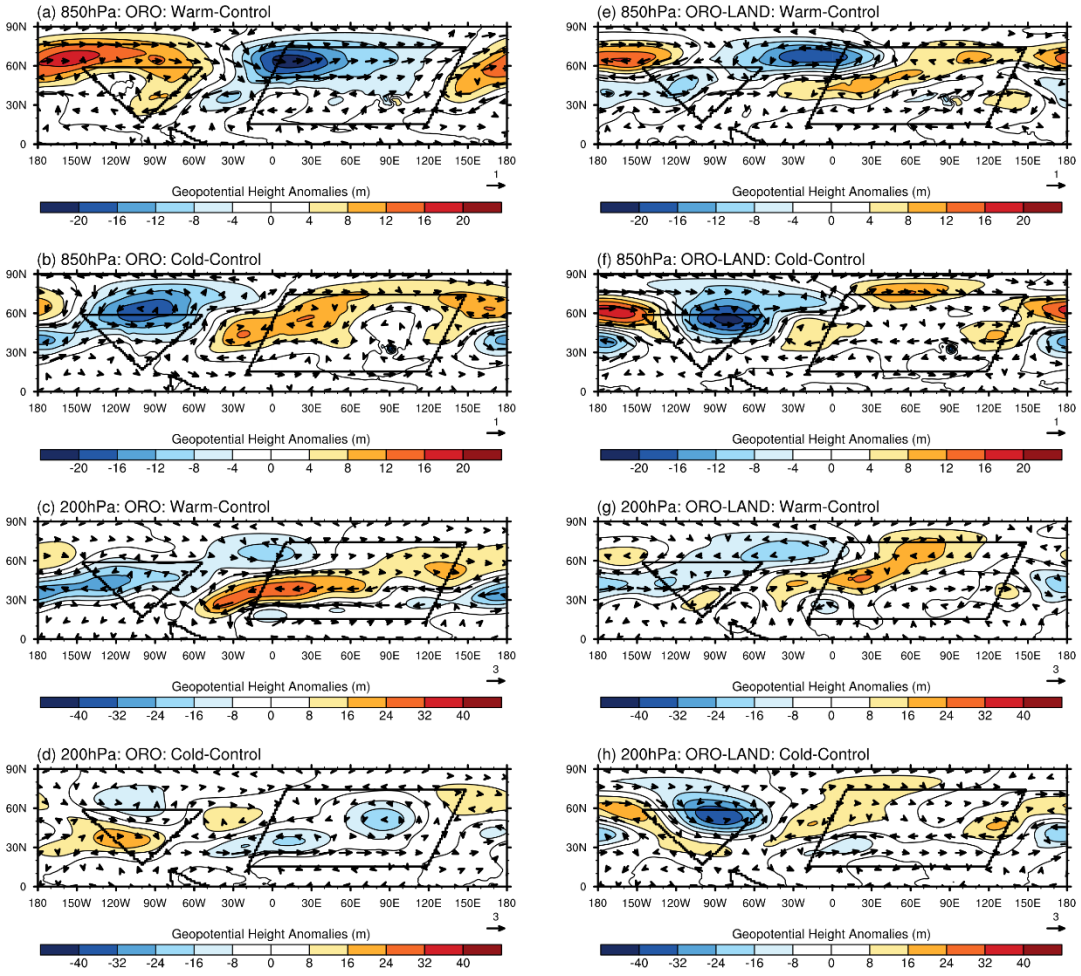

Figure 3.11: Same as Fig. 3.7, but for the orography experiments. (a-d) are the same as Fig. 3.7a-d, except for the orography experiments, and (e-h) are the differences between the orography experiment and land experiment. Contour interval and reference vectors are (a,b,e,f) 4 m, 1 m s^{-1} and (c,d,g,h) 10 m, 3 m s^{-1}.

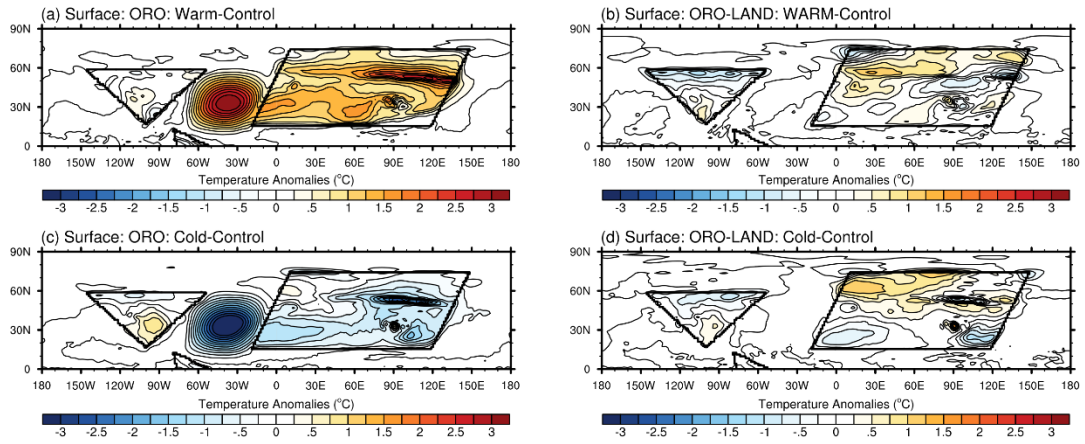

Figure 3.12: Same as Fig. 3.8, but for the orography experiments. (a,c) are the same as Figs. 3.8a and 3.8c, except for the orography experiments and (b,d) are the differences between the orography experiments and land experiments. Units are in degree Celsius (°C) and contour interval is 0.25°C.

CHAPTER 4

NORTH AMERICAN PRECIPITATION RESPONSE

4.1 Precipitation Responses in an Aqua-planet

In the previous chapter, we examined the general circulation response to warm and cold SST anomalies similar to the AMO under aqua-planet, idealized land, and orography conditions. We now apply this overall understanding of the circulation response to the AMO to the specifics of precipitation over North America. We describe the precipitation anomalies forced directly by the SST anomalies, as well as the responses to land and orography and determine how the interactions of these forcings alter precipitation over North America in response to the AMO.

4.1.1 Control SST

We first present the entire hemisphere in order to establish the global precipitation response before focusing on the North Atlantic and North America. The mean precipitation for the Northern Hemisphere in the aqua-planet simulation is shown in Fig. 4.1a. As one would expect, the precipitation response is essentially a function of latitude, and is consistent with the zonally symmetric general circulation discussed in Chapter 3 (Fig. 3.1). In the tropics, there is strong precipitation associated with the intense convection of the Inter-tropical Convergence Zone (ITCZ). To the north in the subtropics, the high pressure belt and widespread subsidence associated with the descending branch of the Hadley Cell largely inhibits precipitation, even with abundant moisture from the ocean surface. In the mid-latitudes, there is greater precipitation,

consistent with the realistic location of the mid-latitude storm track. North of the mid-latitudes, precipitation weakens. An important note from Fig. 4.1a is that the pattern and magnitude indicate that the model is capable of producing realistic precipitation even with the highly altered model surface boundary. This gives us confidence in examining the relationship between the circulations (discussed in Chapter 3) and the precipitation and precipitation processes over North America discussed here in the current chapter.

4.1.2 Warm SST Anomaly

When the warm and cold SST anomalies are introduced into the realistic location of the North Atlantic (Figs. 4.1b and 4.1c, respectively), the strongest response is, unsurprisingly, over the SST anomaly region. With the warm SST anomaly, a large positive precipitation anomaly occurs over the North Atlantic, reasonable considering the large increase in evaporation and surface temperature that occurs with the increase in SST. The warmer and moister near-surface air decreases the stability over the heating region, leading to enhanced convection over the North Atlantic. Upstream from the anomalously warm SST in the North Atlantic, a narrow band of negative anomalies is oriented north-south throughout most of the subtropics and mid-latitudes (between 60°-90°W). This may be due to a stabilizing effect of upper-level heating from the convection center that extends upstream from the SST anomaly region and suppresses precipitation development immediately upstream.

The suppression of precipitation continues much further upstream in the mid-latitudes. North of about 35°N latitude, there are negative precipitation anomalies over much of the area that would contain the realistic North American continent. This is

interestingly consistent with the precipitation results in the more realistic summertime simulations of Hu et al. (2011), and spring and summer simulations of Wang et al (2010), despite the differences in land surface and season. In Fig. 3b of Hu et al. (2011) and Fig. 1c of Wang et al. (2010), there is decreased precipitation during the warm phase of the AMO north of 30°N latitude throughout much of their domain, including over the northwestern North Atlantic. These similarities suggest that the warm North Atlantic SST can have a notable effect in the mid-latitudes upstream, even without any contribution from land processes.

In the subtropics, there is a weaker band of positive precipitation anomalies upstream of the warm SST anomaly. Comparisons of Figs. 4.1a and 4.1b show that the subtropical anomalies are about 5-10% of the mean and suggest that the subtropics may be more vulnerable to AMO-forced precipitation variations than the mid-latitudes. Furthermore, the north-south stratification of the anomalies presented in Hu et al. (2011) is likely a robust feature directly forced by the warm SST anomalies, even if the details may vary (as we present later in this chapter).

4.1.3 Cold SST anomaly

The upstream precipitation response to the cold North Atlantic SST anomalies (Fig. 4.1c) is of opposite sign, but far weaker than the warm SST response. As with the warm SST response, the greatest response is directly over the SST forcing region, where there is a notable decrease in precipitation. The decreased temperature and moisture available near the surface likely increases the atmospheric stability and reduces convection over the North Atlantic. However, the magnitude of the anomalies is weaker

with the cold SST anomaly than with the warm SST anomaly. If we consider the Clausius-Clapyeron relationship, the reason for the nonlinearity becomes clear. A reduction in temperature reduces the atmospheric moisture content by a lesser amount than a similar increase in temperature can increase the moisture. This relationship may help start explaining the weaker overall precipitation anomalies to the cold SST anomaly.

Immediately upstream of the SST forcing region, there is a slight hint of a north-south oriented positive anomaly reminiscent of the negative anomaly from the warm SST case. Further upstream of the SST forcing, the precipitation anomalies become weaker and more diffuse, and there is no strong precipitation pattern over the latitudes and longitudes of North America. A lack of definite pattern, relative to the warm SST case, and having both negative and positive anomalies is similar to previous studies of the cold phase of the AMO in spring and summer (Wang et al. 2010; Hu et al. 2011).

4.2 Atmospheric Forcing on Precipitation in an Aqua-planet

We next explore possible sources of the precipitation anomalies. Temperature variations and atmospheric moisture content appear to play a dominant role in the local response over the SST anomaly (Figs. 4.1b and 4.1c), but the remote connections upstream are less obvious. To better understand these remote connections, an analysis similar to that of Brayshaw et al. (2008) is used. We examine the changes in atmospheric baroclinicity and the storm track forced by the SST anomalies. By applying this type of analysis to the circulation anomalies presented in Chapter 3, it becomes possible to understand how the circulation changes forced by the North Atlantic SST anomalies are able to alter upstream precipitation. For the remainder of this chapter, we will focus on

North America and the North Atlantic exclusively. Therefore, all figures starting with Fig. 4.2 will be limited to 10°N to 70°N latitude, and 180°W to 20°E longitude.

4.2.1 Storm Track

The storm track can be identified by examining the geopotential height variance at 850 hPa (Fig. 4.2a). Daily data were band-pass filtered to extract only the disturbances with a period of 2 to 6 days, the typical period of mid-latitude synoptic systems, and the variance was calculated from the filtered data. The statistical variance is calculated with

$$s^2 = \frac{1}{n-1}\sum_{i=1}^{n}\left(Z850_i - \overline{Z850}\right)^2 \quad (4.1)$$

In (4.1), n is the number of days in model years 3-20 (i.e., 6570), $Z850_i$ is the i^{th} daily observation and $\overline{Z850}$ is the mean across all days. A similar process has been used in previous studies (e.g., Brayshaw et al. 2008). An enhanced, weakened or shifted storm track manifests as greater, lesser or displaced variances, respectively. More specifically, high variance indicates that there is either a greater magnitude or a greater frequency of synoptic-scale disturbances at that location and that the storm track is stronger. The opposite occurs with a reduction in variance, where decreased variance indicates a weak storm track, with smaller storm magnitudes or more infrequent storms.

From Fig. 4.2a (note the reduced domain), it is clear that the majority of the variance occurs poleward of 40°N latitude, with some variance extending south toward 30°N. This is consistent with the location of the mid-latitude storm track along the polar front. Due to the aqua-planet surface boundary and surface homogeneity, the storm track is zonally symmetric. The precipitation in Fig. 4.1a agrees well with the storm track

location and indicates that the storm track can be an important control on mid-latitude precipitation.

When the warm SST anomaly is included in the model, there is a notable change in the storm track (Fig. 4.2b). Over the SST anomaly region, there is a strong increase in the storm track, consistent with the results of Brayshaw et al. (2008), who found that the storm track intensifies over and downstream of warm SST anomalies. This is due to the increase of the mid-latitude SST and atmospheric temperature gradients. The increased temperature gradient enhances the vertical shear of the horizontal wind and the baroclinicity. In contrast, the storm track weakens upstream of the SST anomaly region west of 60°W longitude, a result suggesting that the polar front is weaker for a considerable distance upstream of the warm SST forcing. Furthermore, comparisons with Fig. 4.1b show that the changes in the storm track agree well with the precipitation anomalies.

In response to the cold SST anomaly (Fig. 4.2c), a pattern in the variance opposite to the warm SST response is generally found. Over the cold SST anomaly, a weakening of the storm track is forced by a decrease in the temperature gradient and a resulting decrease in baroclinicity and storm development. Upstream of the SST forcing, the storm track is generally stronger than in the control experiment, suggesting that the polar front is stronger and that there is increased synoptic activity along the front.

The position and intensity of the storm track along the polar front are important in determining how the AMO affects mid-latitude precipitation. To understand the changes along the polar front, we need to examine the positions and magnitudes of the jet streams, particularly the mid-latitude jet. The strength and position of the mid-latitude jet is a

fundamental component of the mid-latitude storm track, since the jet is positioned along the strongest geopotential height (and thus, mass) gradients in the mid-latitudes. Along this boundary, the polar front serves as a major source of instability for synoptic-scale disturbances that pass through an area. We can examine the extent of the disturbances by looking at the mean and anomalous zonal wind at 300 hPa (Figs. 4.3a-c). This level is particularly useful, as both the subtropical and mid-latitude jets can be seen to some extent (Fig. 4.3a). Identifying both jets is crucial, as there can be times in which the two jets may be merged and other times in which a split jet may exist. Whether the jets are split or not can change the latitude at which the storm track from the Pacific Ocean enters North America (e.g., Barton and Ellis 2009). In a cross-section of the average zonal wind between 80°-120°W longitudes (Fig. 4.3d), it appears that jets are split and that the latitudes of the subtropical and mid-latitude jets are at about 25°-30°N and 40°N, respectively.

4.2.2 Zonal Winds

In Chapter 3, we described a weakening of the mass (i.e., pressure) gradient throughout the entire troposphere in response to the warm SST anomaly in the mid-latitudes over the North American latitudes and longitudes (Figs. 3.3a and 3.3c). Because of the west-east orientation of the height anomalies, there is extensive weakening of the mid-latitude zonal winds upstream of the SST forcing (Fig. 4.3b). The negative zonal wind anomalies at 40°N (Fig. 4.3e) are near the position of the mid-latitude jet between 40°N-50°N (Fig. 4.3d) and indicate that while the mid-latitude jet weakens, it does not shift much away from its climatological (i.e., control) position of around 40°N-50°N

(Fig. 4.3d). Another way to look at the zonal wind anomalies is to say that the weakening of the zonal wind in the mid-latitudes suggests a weakening of the polar frontal boundary. This is consistent with the extensive high latitude positive geopotential height anomalies shown in Figs. 3.3a and 3.3c, suggesting a weakening (i.e., warming) of the polar air masses and polar front.

The response of the zonal wind to the cold SST anomaly (Fig. 4.3c) is notably different from the response to the warm SST anomaly (Fig. 4.3b). Overall, the magnitude of the upstream anomalies in the mid-latitudes is weaker than with the warm SST anomaly, and is forced by the weak upstream response in geopotential heights with the cold SST anomaly (Figs. 3.3b and 3.3d). Upstream of the SST anomaly region, the positive zonal wind anomalies between 40°-60°N suggest that the mid-latitude jet may shift northward and/or may become slightly enhanced (Fig.4.3f). In addition, the geopotential height anomalies in Fig. 3.3b suggest that there is a warming in the mid-latitudes and cooling of the high latitudes which forces a northward retreat of the polar air mass. This in turn, drives the changes in the mid-latitude jet.

4.2.3 Baroclinicity

It was mentioned earlier that changes in the temperature gradient and baroclinicity over the SST anomaly region are important in modifying the storm track. The thermal wind relation indicates that stronger horizontal gradients of temperature is critical in the development of baroclinic instability. From this, it becomes apparent that jet anomalies forced by changes in the meridional temperature gradient in response to the warm or cold SST anomalies can have a strong impact on the precipitation through modification of

atmospheric baroclinicity. In other words, any regions of increased or decreased upper tropospheric winds can have a strong impact on baroclinic development and the storm track. To this end, we look at a direct measure of baroclinicity, the Eady maximum growth rate (Fig. 4.4; e.g., Charney 1947; Eady 1949; Hoskins and Valdes 1990; Keyser and Anthes 1982). The dimensionless Eady growth rate is strongly dependent upon the wind shear between two atmospheric levels and is given as

$$\sigma = 0.31f \left|\frac{\partial \boldsymbol{V}}{\partial z}\right| N^{-1} \tag{4.2}$$

In (4.2), f is the Coriolis parameter, $\boldsymbol{V}$ is the wind speed and z is the geopotential height. N, the Brunt-Väisälä frequency, is defined (after a slight alteration) in Keyser and Anthes (1982) as

$$N = \left[\frac{g}{\theta_o}\frac{\partial \Theta}{\partial z}\right]^{\frac{1}{2}} \tag{4.3}$$

In (4.3), g is the gravitational constant, θ_o is the potential temperature at 1000 hPa and Θ is the potential temperature. Here, the partial derivatives in (4.2) and (4.3) are calculated as finite differences between two pressure levels. In order to determine the changes in baroclinic growth throughout much of the troposphere, we use similar levels to Brayshaw et al. (2008), who examined baroclinic growth anomalies between 925 hPa and 775 hPa (lower troposphere) and 925 hPa and 250 hPa (whole troposphere). In order to determine the changes in baroclinic growth throughout much of the troposphere, we use 925 hPa and 250 hPa as our levels.

We see in Fig. 4.4a that the mean baroclinicity for the aqua-planet experiment is strongest along the subtropical jet stream. This is unsurprising considering the substantial differences in the zonal wind speed between the upper and lower troposphere at that latitude. The high growth rate region extends toward the mid-latitudes to about

60°N and includes the latitudes where the mid-latitude jet and polar front occur. It is in this region that precipitation from baroclinic disturbances occurs (Figs. 4.4a vs. 4.1a).

When the warm and cold SST anomalies are introduced (Figs. 4.4b and 4.4c, respectively), the upper tropospheric wind anomalies (Figs. 4.3b and 4.3c) are the dominant control on baroclinic variability. This is due to small magnitude of the lower tropospheric zonal wind anomalies compared to upper tropospheric winds (Figs. 4.3e and 4.3f). In Fig. 4.4b, the effect of the weakened mid-latitude jet upstream of the warm SST anomalies can be seen. West of 60°W longitude, there are negative baroclinic anomalies in the mid-latitudes that intensify with greater distance from the SST forcing. In the subtropics, the intensified subtropical jet enhances the Eady growth rate upstream of the SST forcing. The precipitation anomalies in Fig. 4.1b agree quite well with these baroclinic anomalies. Such agreement indicates that the weakening of the mid-latitude jet and resulting decrease in baroclinicity serve as strong controls on the precipitation.

Similar to the response to the warm SST anomaly, the response of the Eady growth rate to the cold SST anomaly (Fig. 4.4c) closely mirrors the upper tropospheric zonal wind anomalies in Fig. 4.3c. The enhancement/northward shift of the mid-latitude jet between 60°-120°W acts to increase the baroclinicity north of 40°N latitude. West of 90°W and south of 40°N, most of the mid-latitudes experience a decrease in baroclinicity. The significant positive Eady growth rate anomalies are fairly limited in extent, as are the strong negative anomalies. There is a much greater area of weak or neutral anomalies when compared to the baroclinic growth anomalies in response to the warm SST anomaly. A lack of strong magnitudes are likely a source of the weaker precipitation

anomalies in response to the cold SST anomalies (Fig. 4.1c). Regionally however, the Eady growth rate anomalies can be large enough to potentially be important.

These baroclinic anomalies are important because they help develop or amplify passing synoptic-scale disturbances. Enhancement of the baroclinicity allows storms to intensify, whereas weaker baroclinicity prevents or reduces storm development. The forcing for the precipitation anomalies in the warm SST case can be summarized as follows: There is a weakening of the upper tropospheric zonal wind in response to a decrease in the polar air mass intensity and decreased temperature gradient. As a result, there is a decrease in baroclinicity upstream of the SST forcing and a decrease in storm development along the polar front. The storm track is not meridionally displaced, but is simply weaker and helps explain why the magnitudes of the precipitation anomalies in the mid-latitudes are relatively strong and uniformly negative upstream of the SST forcing.

In response to the cold SST anomalies, the magnitude of the zonal wind anomalies are weaker than the response to the warm SST anomaly, and are a likely reason for the neutral precipitation anomalies in the mid-latitudes (Fig. 4.1c).

4.3 Precipitation and Storm Track Responses with Continents

As in Chapter 3, we next include idealized representations of North America, South America and Eurasia in the model, and examine how land without orography can modify the precipitation response to the symmetrical SST. We are also interested in how the continents further modify the precipitation response to warm and cold SST anomalies

in the North Atlantic. Recall from Chapter 3 that these experiments are referred to as the "land experiments."

4.3.1 Control SST

Figure 4.5a shows the precipitation response to the control SST with idealized continents, and Fig. 4.5d shows the difference between the idealized continent experiment and the aqua-planet experiment with the control SST (Fig. 4.1a). Examining Fig. 4.5d, several important changes from the aqua-planet run are evident. Over the North Atlantic, there are three major features in the precipitation anomalies. The first is an extensive region of decreased precipitation in the southeast North Atlantic, off the Eurasian coast and extending eastward into the continental interior. This is likely due to a stabilization of the atmosphere from advection of warm and dry air from Eurasia by the lower tropospheric trade winds (Chapter 3; Figs. 3.4c and 3.5c). Furthermore, the intensification of the high pressure over the North Atlantic and the formation of the North Atlantic high pressure (NASH) both increase subsidence over the region (Figs. 3.5b and 3.5d), particularly over the eastern part of the North Atlantic basin. These lead to a much weaker precipitation signal over the southeastern North Atlantic.

In the mid-latitude North Atlantic, there is a notable increase in precipitation between the two continents. There is essentially no extension of the positive anomalies westward onto North America, suggesting that the anomalies originate over the ocean and then are advected by the mid-latitude westerlies. In the southwestern North Atlantic, there is also an increase in the precipitation. In this region, we see the effect of the lower tropospheric southerly flow anomalies presented in Fig. 3.4c. The anomalous southerly

flow transports heat and moisture poleward. This influx of lower-latitude air increases the temperature and moisture content of the air, decreasing the stability over the region and partially overcoming the stable atmosphere forced by the subtropical high pressure belt.

Over North America, there is an overall reduction of the precipitation throughout much of the continent, compared to the same location in the aqua-planet run. This is unsurprising, considering the large decrease in moisture availability over land compared to the all-ocean surface of an aqua-planet. The strongest decreases in precipitation are found in the southern part of the continent (Fig. 4.5a). This region broadly corresponds to the realistically drier areas of the southwest U.S. and northern Mexico.

In the mid-latitudes, the drying effect of the continent is not as strong (Fig. 4.5d). Off the west coast of North America, there is a strong increase in precipitation in the subtropics and lower mid-latitudes. The positive precipitation anomalies extend onshore slightly between 30°-50°N and then reverse sign, before extending across the northern part of the continent as weaker negative anomalies. The anomalies extend into the North Atlantic, becoming strong positive anomalies again, but farther to the north than the Pacific anomalies. The smaller magnitude negative precipitation anomalies over North America are partially due to the mean flow from the North Pacific Ocean. Moist low-level air from the North Pacific is advected eastward into the continental interior by the mid-latitude westerlies, unimpeded due to the lack of orography.

The storm track displays strong intensifications over the oceans and marginal changes over North America (Fig. 4.6d), and is consistent with the precipitation anomalies in Fig. 4.5d. In the North Pacific, the storm track intensification is strong to

the south of the aqua-planet position and acts to shift the storm track to the south. In the North Atlantic, the opposite occurs. Intensification of the North Atlantic storm track occurs to the north of the aqua-planet location, indicating a northward shift in the storm track in the land experiment. Enhancement of the storm track in the North Pacific reasonably agrees with the established location of the observed spring storm track (Chang et al. 2002). The storm track then weakens over the continental interior but intensifies again over the North Atlantic at a higher latitude. Chang et al. (2002) found a similar pattern in observations. It is worth noting that, in our simulations, the storm track in both ocean basins occurs at slightly higher latitudes than in the observations in Chang et al. (2002). The differences are small however, and the relative latitudes of the storm tracks between the ocean basins are similar. These results suggest that the model is capable of describing a relatively realistic storm track with only idealized continents. Furthermore, they may indicate that a simple land-ocean contrast is sufficient in forcing the bulk features of the observed storm track.

Zonal winds exhibit a strong change over North America in the land experiment, and are consistent with the precipitation and storm track anomalies. Comparisons of Figs. 4.3a to 4.7a and 4.3d to 4.7d suggest that the mid-latitude and subtropical jets are merged over the North Pacific Ocean and North America. This change is indicated by the intense strengthening of the zonal winds between the positions of the two jets in the aqua-planet run (Figs. 4.8a and 4.8d). The merged jet extends over North America and then tilts southwest to northeast along the east coast of North America (Fig. 4.7a). This change in jet pattern over North America supports the conclusions in Brayshaw et al. (2009), who found that when land was included in their model, the jet experienced a

similar southwest to northeast tilt. When a more realistic North American continent was used (similar to the one used in this study), the tilted jet was amplified due to the orientation of the coastline. This is also consistent with observations regarding the observed jet pattern in the western hemisphere (Nakamura et al. 2004), and stresses the importance of not only the basic continental influence, but also of the shape of the coasts in determining the jet structure.

Over North America, the increased meridional temperature gradient from continental heating in the south and cooling in the north (Fig. 3.5c) weakly increases baroclinicity between 30°-40°N (Fig. 4.9d). The strengthening of the temperature gradient likely intensifies the merged jet across the continent and the thermal wind. It is interesting that the atmosphere is more baroclinic south of 40°N and, despite this, there is a significant decrease in precipitation in the southern half of the continent. The reason for this is the absence of adequate surface moisture. In the subtropics, the mean flow is much weaker than in the mid-latitudes. Therefore, moisture transport from the oceans is weak and there is little to compensate for the loss of a local moisture source. Without a moisture source, precipitation is unable to develop, even in an otherwise favorable environment.

4.3.2 Warm SST Anomaly

We now investigate how land modifies the precipitation response to the warm and cold SST anomalies. It is immediately apparent from comparing Fig. 4.5b to Fig. 4.1b, that land does little to alter the pattern of the precipitation response to the warm North Atlantic SST anomalies. The land modification of the warm SST response (Fig. 4.5e) is

very similar to the direct response to the warm SST anomaly in the aqua-planet experiment. This should be expected considering that the land effect is generally weak compared to the direct response to the warm SST anomalies (Chapter 3; Figs. 3.3a vs.3.7e). However, the expansion of the high pressure over North America in the presence of land further decreases precipitation in the mid-latitudes. There is also an increase in precipitation along the northern edge of the continent. Figure 4.6e shows that there is further weakening of the storm track in the mid-latitudes and is a likely cause for the additional decrease in precipitation. This reinforcement of the direct response to the warm SST anomaly, though small, is important in maintaining the precipitation anomalies.

Further decrease in mid-latitude storm track intensity in the warm SST anomaly case is fueled by additional weakening of the upper tropospheric zonal winds between 30°-40°N and a weaker polar front. Figures 4.7b and 4.7e show the zonal wind response to the warm SST anomaly in the presence of land, and Figs. 4.8b and 4.8e show the modifications of that response forced by land. We can see from comparing these figures, that the zonal wind anomalies are similar to the direct (i.e., aqua-planet) warm SST anomaly forced response and that the zonal winds further weaken (Fig. 4.7e). Weakening of the jet in the mid-latitudes limits storm development along the polar front by further decreasing the baroclinicity over North America (Fig. 4.9e). One effect of this change is to further decrease precipitation in the mid-latitude continental interior (Fig. 4.5e).

4.3.3 Cold SST Anomaly

Unlike the modification of the precipitation response to the warm SST by land, where the change is generally an enhancement, the response to the cold SST anomaly in the land experiment changes significantly from the direct response to the cold SST anomaly in the aqua-planet experiment (Figs. 4.5f vs. 4.1c). This is again consistent with the large overall modifications to the cold SST response forced by land discussed in Chapter 3. Over North America, there are extensive areas of increased precipitation in the mid-latitudes and decreased precipitation the southern part of the continent. This modification makes the response to the cold SST anomaly resemble the spatial pattern of the response to the warm SST, but with opposite sign (Figs. 4.5b vs 4.5c), suggesting that land has a strong influence on the observed response to the cold phase of the AMO.

The alteration of the storm track response to the cold SST anomaly (Fig. 4.6f) resembles, though of opposite sign, the change in the response to the warm SST anomaly forced by land (Fig. 4.6e). Upstream of the cold SST anomaly region, there is additional intensification of the North Pacific storm track along the polar front relative to the aqua-planet experiment (Fig. 4.2c). The additional increase in the storm track appears to be sufficient enough that organized precipitation anomalies are able to develop (note the similar magnitudes of the anomalies in Figs. 4.6b and 4.6c).

We can get a better idea of the source of the precipitation and storm track anomalies by comparing them to the geopotential height anomalies (Figs. 3.7c and 3.7g). In Chapter 3, we discussed a dipole height anomaly along the northern edge of North America, negative in the northwestern corner and positive in the northeastern corner. The low pressure center and the intensified storm track suggest an enhancement of storm

development in the eastern North Pacific. Storms that develop in that region are stronger and/or more frequent. These storms then propagate eastward under the westerlies, bringing greater precipitation to the west coast and interior of the continent.

Analysis of the zonal wind and baroclinic anomalies supports this idea. Figure 4.7c shows stronger mid-latitude zonal winds off the west coast of North America and suggests that the merged jet shifts northward in response to the cold SST anomaly. With a stronger and better defined jet off the west coast, the region has increased baroclinicity that aids the growth of disturbances (Fig. 4.8c). In addition, the more northerly position of the jet steers disturbances farther to the north than in the control (symmetric SST) case, enhancing the storm track along the polar front and increasing precipitation in the northern part of the continent (Fig. 4.5c).

Conditions downstream from the storm development region are not as favorable, however, for maintaining the storms over the eastern part of the continent. Zonal wind (Fig. 4.7c) and baroclinic (Fig. 4.9c) anomalies are both weaker, helping weaken the storms propagating eastward across the mid-latitudes. In addition, the positive geopotential height anomalies help deflect the storm track farther to the north in the eastern part of the continent. This gives the storm track (Fig. 4.6c) a southwest to northeast slant in the center of the continent and reduces the influence of the storm track over the eastern side of the continent. Less favorable conditions over the continent suggest that advection of storms from the west is essential to the positive precipitation anomalies in the continental interior. The out-of-phase relationship between the storm track and baroclinic anomalies supports this proposition (Fig. 4.6c). As storms move across the continent, they weaken in the less favorable environment, and the mid-latitude

storm track anomalies weaken toward the east. However, the weakening does not occur instantly and the storm track still remains enhanced farther into the continental interior prior to weakening.

In summary, modifications by land of the response to the AMO-like cold SST anomaly is stronger than the modifications of the response to the warm SST anomaly. Generally, land augments the direct forcing to the warm SST anomaly, but doesn't strongly change the pattern. In contrast, there is a much larger difference in the anomaly pattern in response to the cold SST anomaly. Previous studies have shown the springtime response is generally weak (Wang et al. 2010; Nigam et al. 2011), and that the anomalies just described may be stronger than those shown in other studies, particularly in response to the cold phase of the AMO. Therefore it is important to keep these responses in perspective.

4.4 Precipitation and Storm Track Responses to Continents and Orography

4.4.1 Control SST

The changes in precipitation are quite different when idealized representations of the Rocky Mountains, the Alps and the Tibetan Plateau are included in the model (Fig. 4.10d). In Fig. 4.10a, we see that the precipitation pattern in response to orography is relatively similar to the land without orography response (Fig. 4.5a), but the magnitude is generally smaller. Most of the subtropics has increased precipitation and most of the mid-latitudes has decreased precipitation in response to the orographic forcing when compared to the land experiment (Fig. 4.10d). The main exception in the mid-latitudes is the development of strong dipole of precipitation anomalies on either side of the Rockies.

On the windward side, strong orographic uplift of the mean westerly flow from the Pacific Ocean enhances precipitation. On the lee side, a strong rain shadow effect occurs due to the loss of moisture along the windward side of the mountains. In the southern part of the continent, there is a strong increase in precipitation, particularly along the east coast. In Chapter 3, we described a cyclonic circulation anomaly along the southern edge of North America (Figs. 3.9c and 3.10d). This anomalous circulation brings warm, moist air into the southern part of the continent and provides moisture for the increased precipitation. The increased precipitation from orography in the south partially reverses the precipitation decrease forced by the continent in the land experiment (Fig. 4.5d).

Precipitation in the central part of North America is reduced to an amount similar to that found in spring observations (Higgins et al. 1997). The weakest precipitation occurs in the lee of the Rockies and then increases toward the east coast of North America. This is because the moist flow into the continental interior from the North Pacific is obstructed by the Rockies, and the southerly flow along the western flank of the NASH becomes largely responsible for moisture transport. The precipitation amount is smaller than that found in the summertime results of Hu et al. (2011) and Higgins et al. (1997), presumably because the NASH and GPLLJ are not as well formed during spring (Seager et al. 2003; Weaver and Nigam 2008). A similar reduction in the southerly flow into the North American interior can be seen in the idealized simulations (Fig. 3.9a). Not only does this help support the previous understanding of the observed seasonality in the NASH and GPLLJ, it also reinforces the important role of orography in producing these features and the precipitation that results from them. Ting and Wang (2006) found that the Rockies were critical in establishing the GPLLJ and observed precipitation patterns in

the continental interior. In the present study, we show that even idealized representations of the Rockies are sufficient in forcing a semi-realistic GPLLJ and precipitation. Therefore, the finer features of the realistic Rocky Mountains are not as important as the gross structure of the mountains in forcing the observed patterns of circulation and precipitation over the central U.S.

The decreases in mid-latitude precipitation that occur in the orography experiment are also due to a large decrease in the storm track (Fig. 4.11d). Immediately downstream of the Rockies, there are decreases of about 30-40% in storm track intensity over the continental interior. The decrease in storm track extends well beyond this region, though at reduced magnitude, and largely counters the increase in storm track forced by the continent itself (Fig. 4.6d). Overall, the storm track is weakened more by orography than it was enhanced by the continent. The net result from both effects is a relatively unchanged mid-latitude storm track over the oceans, and a weaker storm track over North America. An exception to the weaker storm track is along the southern boundary of the Rockies, where the storm track is stronger, though in a limited area. This is consistent with the observed storm development region on the lee side of the Rockies. Storms develop in this region and then propagate to the east or northeast where they interact with increased lower tropospheric moisture from the south and result in increased precipitation in the southeastern part of the continent (Fig. 4.10d).

The reason for the storm track changes is likely from additional alterations of the jet stream magnitude and location, and changes in baroclinicity. In Chapter 3, we described a strong decrease in the speed of the mid-latitude westerlies from mountain and frictional torques. This can be clearly seen in the mean zonal wind with orography (Figs.

4.12a and 4.12d) and the differences from the land without orography case (Figs. 4.13a and 4.13d). Over and east of the Rockies, there is a strong weakening of the zonal flow throughout the troposphere (Fig. 4.13d). In contrast, the zonal wind is increased in the subtropics and tropics. We can see in Fig. 4.12d that inclusion of the Rocky Mountains splits the single jet found in the land experiment (Fig.4.7d). The subtropical branch is greatly enhanced, and flows along the southern edge of the Rockies, while a much weaker mid-latitude branch shifts far to the north and along the northern side of the Rockies (Fig. 4.12d). The zonal flow is weakened the most across the mountains (near 40°N). As a result, storms from the Pacific Ocean enter the continent either farther to the south or north, and much of the mid-latitudes are excluded from the North Pacific storm track. An added effect of the split jet is that the subtropical jet passes through the storm development region in the lee of the Rockies and assists in the propagation of the storms toward the east.

Another way of looking at the zonal wind anomalies is from the perspective of the mass and temperature distributions. It is well-known that mid-latitude orographic features increase the poleward eddy heat flux (e.g., Peixoto and Oort 1992). In Chapter 3, we discussed how an increase in the geopotential heights in response to orography indicated strong warming in the high-latitudes (Figs. 3.9c and 3.9d) compared to the land without orography experiment. Strong polar warming weakens the meridional temperature and pressure gradients in the mid-latitudes, and reduces the zonal wind speeds. When combined with the mountain and frictional torques, there is a strong reduction of the zonal winds in the mid-latitudes.

The intensification of the southern branch of the jet over North America increases the baroclinicity over the southern part of the continent (Fig. 4.14d). This region of stronger baroclinicity overlaps with the lee side cyclogenesis area forced by the orography, and thereby provides additional instability needed for development of the stronger storm track to the south (Fig. 4.11d). To the north, the mid-latitudes have a strong decrease in baroclinicity from the weaker mid-latitude jet. However, this decrease in baroclinicity is mitigated by the overall spatially uniform weakening of the mid-latitude westerlies throughout the entire troposphere (Fig. 4.13d). These changes help to maintain most of the vertical shear (and baroclinicity) from the land experiment (Fig. 4.14a vs. 4.9a). As a result, the combined baroclinic response to both land and orography is negative and reduced from the zonally symmetric aqua-planet experiment (Fig. 4.4a).

4.4.2 Warm SST Anomaly

The modification by orography on the precipitation response to the warm SST anomalies (Fig. 4.10e) is much different from both the aqua-planet response (Fig. 4.1b) and the modifications by land (Fig. 4.5e). Inclusion of orography reverses many of the negative precipitation anomalies in the mid-latitudes forced by the warm SST anomaly, and further amplified by the continent. The net result is much weaker negative precipitation anomalies in the mid-latitudes and even some limited areas displaying weak positive anomalies (Fig. 4.10b). In the southern, subtropical part of North America, there is a slight reduction of the positive precipitation anomalies. However, the reversal of the warm SST forced anomalies is much less in the subtropics than in the mid-latitudes.

This overall weakening of precipitation makes the model response more consistent with the relatively weak springtime precipitation anomalies in Wang et al. (2010). In fact, the orographic effect reduces the precipitation anomaly to a smaller magnitude than is found in either Wang et al. (2010) or Nigam et al. (2011). This is likely due to the differences in study design between this study and theirs. However, the large change in response and better agreement with previous studies suggest that the idealized orography reasonably captures the essential characteristics of the realistic orographic modification of the precipitation. In both Nigam et al. (2011) and Wang et al. (2010), the precipitation anomalies in spring are smaller than in summer and fall, a result similar to the present study. The weaker response with orography indicates that it is this modification of the response to the warm SST anomaly that leads to the weaker springtime precipitation response.

We now evaluate how orography weakens the precipitation pattern in response to the warm SST anomaly in the North Atlantic. Figure 4.11e shows that orography forces a stronger storm track in the mid-latitudes over North America compared to the storm track modified by land alone. This result counters the previous storm track anomaly pattern, and produces a weaker negative storm track with orography (Figs. 4.11b vs. 4.6b). The weaker (but still negative) storm track anomalies indicate a nearly neutral, unchanged storm track over North America. As a result of the change from a weak storm track to a neutral one, mid-latitude precipitation increases from very dry without orography to only slightly dry or normal with orography.

Without orography, the mid-latitude jet and atmospheric baroclinicity weakens in response to the warm SST anomaly. We should expect changes in the anomalies of these

fields to be an important component of the increased precipitation and storm track response with orography. This is indeed the case, as the orographic effect strongly increases the zonal winds (Figs. 4.13b and 4.13e) and baroclinicity (Fig. 4.14e) in the continental interior, compared to the land experiment, and reverses the previous pattern of relatively weak mid-latitude winds (Fig. 4.7b vs. 4.12b). One implication of this is that the mid-latitude jet is not weakened as it was in response to the land effect and SST forcing, eliminating the response that led to drier conditions. The stronger mid-latitude winds from the orographic effect are due to greater, rather than weaker, meridional pressure and temperature gradients (Figs. 3.11c and 3.12a). When combined with the opposing pattern from the direct response and land effect, the resultant wind anomaly in response to the warm SST anomaly is weak, and there is little overall change from the mean background flow (Figs. 4.12b and 4.12e).

4.4.3 Cold SST Anomaly

The modification by orography of the precipitation response to the cold SST anomaly (Fig. 4.10c) is also quite different from the land experiment without orography (Fig. 4.5c). With orography, there is no longer an extensive positive precipitation anomaly in the mid-latitudes (Fig. 4.10c). Windward of the Rockies, there is a strong increase in precipitation forced by a stronger low-level flow intruding onto the western side of the continent (Fig. 3.11b). This enhances precipitation from orographic uplift of the moist air. The large differences between Figs. 4.5c and 4.10c indicate that orography strongly modifies the mid-latitude precipitation response during the cold phase of the AMO, just as land heavily modified the direct response to the cold SST anomalies (Fig.

4.5f). This large change due to orography weakens the precipitation anomalies in the continental interior.

Reduction in the fairly strong positive precipitation anomalies can be partially attributed to modifications of the storm track by orography (Fig. 4.11f). The mid-latitude storm track anomalies are slightly weaker with orography, resulting in smaller (but still positive) storm track anomalies in the continental interior (Fig. 4.11c). This is particularly notable in the eastern North Pacific. Here, the storm development region from the land experiment is markedly weaker, due to a weakening and splitting of the offshore low pressure described in the previous section (Figs. 3.11b vs. 3.7b).

There is an interesting matter raised by the storm track and precipitation anomalies. The changes forced by orography cause the precipitation anomalies in the continental interior to become negative in response to the cold SST anomaly, despite a slightly stronger storm track. This is contrary to the patterns discussed previously. To resolve this discrepancy, we need to consider the availability of moisture in the continental interior. Figure 3.11b indicates that extension of the high-latitude low pressure over the North America intensifies the low-level westerlies throughout the continental mid-latitudes (Fig. 4.12f). As a result, the southwest to northeast motion along the western flank of the NASH intensifies, causing two primary effects. First is that the more zonal flow limits the meridional transport of moisture into the continental interior from the south. The moist flow from the south is displaced to the east before it can extend far into the continent, leaving the continental interior under a more continental (i.e., drier) air mass. Second, the enhanced westerly flow along 40°N increases moisture divergence in the continental interior, further promoting moisture loss. Not only is less

moisture being transported into the area, there is more being exported, resulting in weak moisture divergence in the lee of the Rockies. Even with a small increase in the storm track in response to the cold SST anomaly, less moisture is available for precipitation. However, the stronger storm track likely helps to offset some of the precipitation decrease in the continental interior.

Figure 4.13f indicates that orography forces an increase in zonal winds throughout the mid-latitudes over North America in response to the cold SST anomalies. As a result, much of the continental interior experiences increased baroclinicity (Fig. 4.14f). This is similar to the response to the warm SST anomaly, though it is slightly weaker. However, the response over the eastern North Pacific is quite different, where there is a decrease in the zonal winds and a strong decrease in baroclinicity over the North Pacific storm track region. Recall that the land without orography experiments indicated that the North Pacific storm track strengthens in response to the cold SST anomaly, and that these disturbances then propagate over the continental mid-latitudes. By weakening storm development off the west coast of North America, the orographic effect deprives the continental interior of these storms or decreases their intensity. The local increase in storm track intensity over the continent from the increased baroclinicity is unable to compensate for this loss.

The weaker North Pacific storm track may be a significant contributor to the rather unique springtime negative precipitation anomalies during the cold phase of the AMO in Wang et al. (2010). In their study, other seasons have mostly neutral to positive anomalies in the continental interior, but spring has weak negative anomalies. From the current study, we can see that orography weakens the storm track from the strongly

enhanced one in the land without orography case. This alone would likely be sufficient to reduce the magnitude of the positive precipitation anomalies from that of the land experiment. When combined with weaker moisture transport from the south, the precipitation is further reduced. These factors lead to the weak springtime precipitation anomalies during the cold phase of the AMO.

4.5 Chapter Summary and Major Findings

Building upon the general circulation discussion from Chapter 3, we examined the precipitation response in North America. Most of the previous studies on the AMO examine summer or fall precipitation patterns, but neglect any significant consideration of spring precipitation because of the weak anomalies relative to the following seasons. This chapter serves to expand the understanding of the interactions between land, orography, and SST in forcing precipitation anomalies. Furthermore, this chapter explored how the weaker springtime precipitation anomalies discussed in some previous studies come to be.

Unsurprisingly, the precipitation response to the aqua-planet surface boundary and control SST is zonally symmetric (Fig. 4.1a). The strongest precipitation occurs along the ITCZ and the mid-latitude storm track, which is positioned along the mid-latitude jet. In the subtropics, precipitation is weak along the subsiding branch of the Hadley Cell. When land is included, mid-latitude precipitation over North America decreases, while it increases over the North Pacific and North Atlantic Oceans (Fig. 4.5d). This occurs due to changes in the storm track in those regions (Fig. 4.6d). Additionally, the split jet in the aqua-planet simulation is replaced by a single merged and

much stronger jet, enhancing the baroclinicity (Fig. 4.9d). Inclusion of orography acts to split the jet over North America, producing one much weaker jet that is shifted northward (Fig. 4.12d), significantly weakening the mid-latitude storm track (Fig. 4.11d) and precipitation (Fig. 4.10d) over the continental interior. Both land and orography act to weaken precipitation over North America.

In the aqua-planet experiment, spring precipitation decreases in the mid-latitudes and increases in the subtropics upstream of the warm SST anomaly (Fig. 4.1b). When continents are included, the magnitudes of the anomalies are intensified, but the pattern changes little (Fig. 4.5b). This is in contrast to the modification of the response by orography, which alters the response to the warm SST anomaly to a much greater extent (Fig. 4.10e). More importantly, the orographic modification to the precipitation is of opposite sign to the SST forcing, leading to a near total cancelation of the combined SST forcing and land effect, thereby reducing the precipitation anomalies to near zero (Fig. 4.10b). These results suggest that the direct SST forcing and the modification by orography are both important contributors to the precipitation anomalies in response to the warm SST anomalies. The modification by land, on the other hand, is minor in shaping the springtime response to the warm SST anomalies.

During the cold phase of the AMO, the story is quite different. Precipitation anomalies in the aqua-planet experiment are minimal, indicating that there is little direct response to the cold SST anomaly upstream of the North Atlantic (Fig. 4.1c). This changes substantially when land is included in the model (Fig. 4.5c), in which the mid-latitudes have increased precipitation and the subtropics have decreased precipitation. After orography is added to the model, the pattern changes again (Fig. 4.10c). The

positive anomalies in the mid-latitudes weaken to the point that they become negative in certain areas. In the southern part of North America, the negative anomalies are largely unmodified. Unlike the response to the warm SST anomaly, the responses to the cold SST anomaly experiments suggest that the modifications by land and orography are the main determinants of the springtime precipitation during the cold phase of the AMO. The combined effect of the modifications is relatively weak negative precipitation anomalies in the subtropics, with some limited extensions into the mid-latitudes. Similar to the responses to the warm SST anomaly, the precipitation anomalies are largely forced by changes in the mid-latitude jet and baroclinic growth rates. However, low-level moisture availability does play some part in causing the precipitation anomalies, although the overall response is largely determined by the dynamic processes (i.e., wind speeds and baroclinicity).

There is essentially no direct precipitation response to the cold SST anomalies during spring. The overall small anomaly pattern during the cold phase of the AMO is determined by the land and orographic effects, which are largely opposite of each other. In contrast, there is a direct response to the warm SST anomalies that is enhanced by the land effect, but largely reversed by orographic effect. It is this countering effect of orography that is essential to producing the weaker springtime precipitation anomalies.

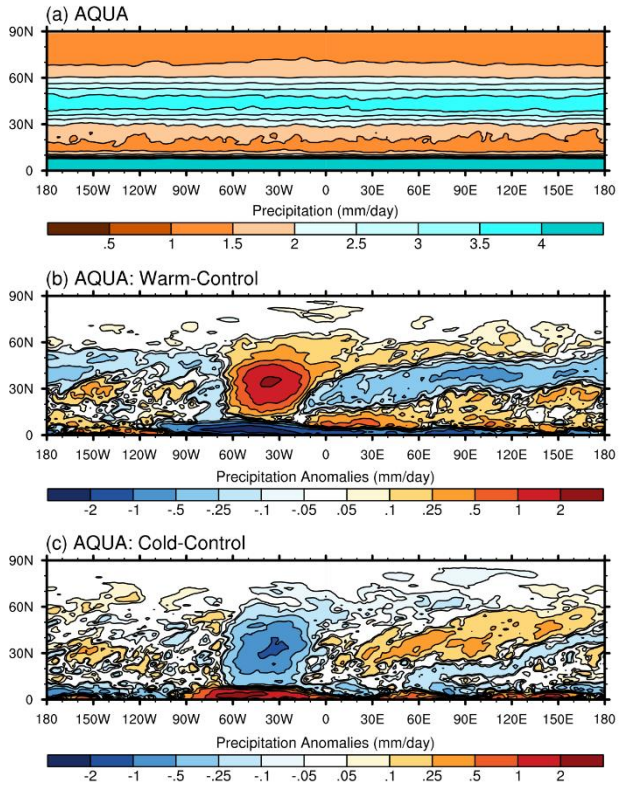

Figure 4.1: Precipitation for the (a) control SST simulation and precipitation anomalies for the (b) warm and (c) cold simulations for the aqua-planet cases. Units are mm day^{-1}.

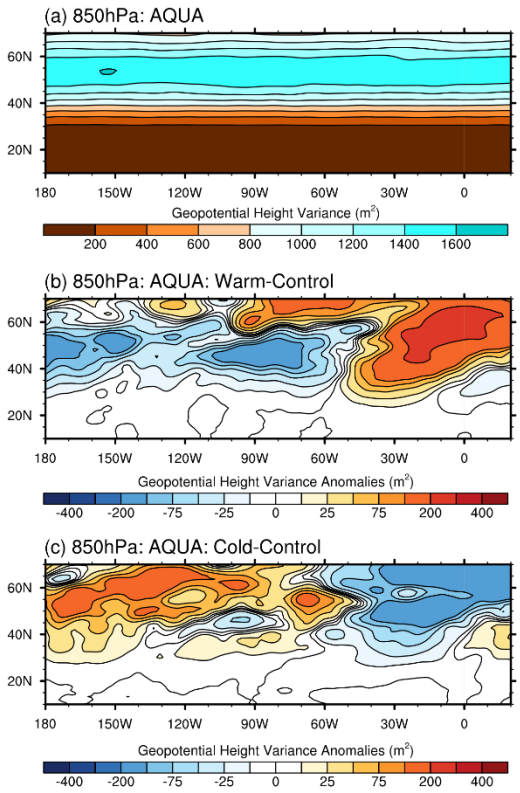

Figure 4.2: Same as Fig. 4.1, but for the variance of the geopotential height at 850 hPa. Units are m^2. Note the reduced domain of the figures. They range from 10°-70°N latitude and 180°W-20°E longitude.

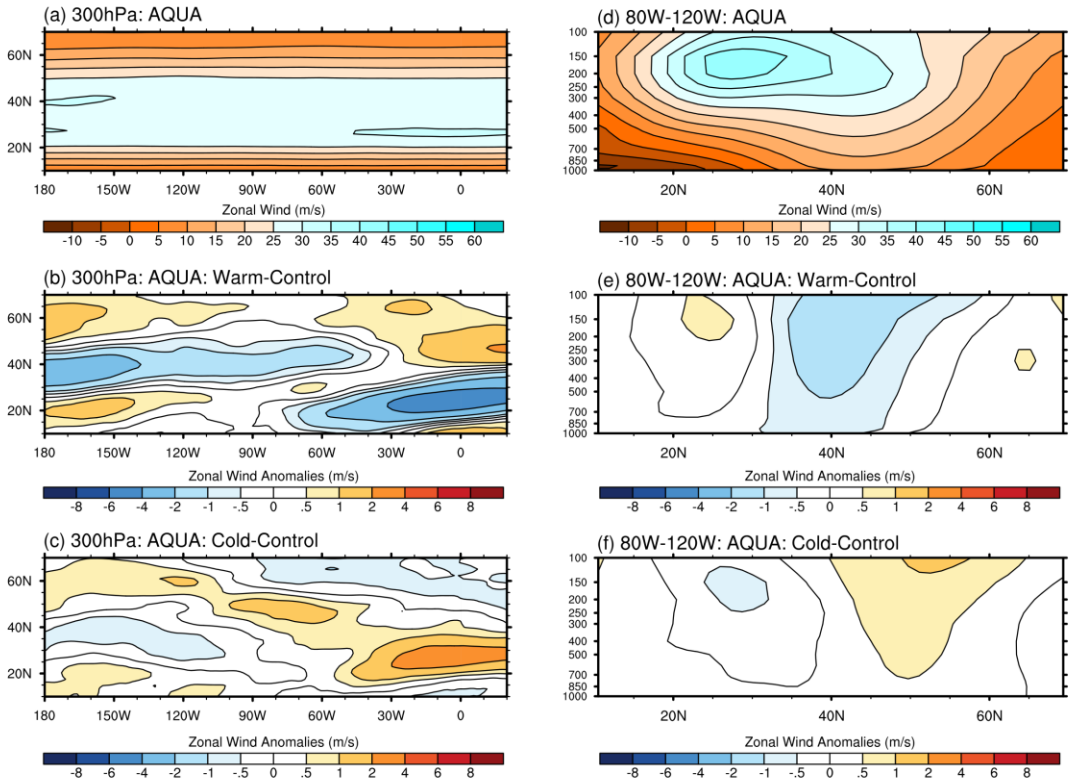

Figure 4.3: (a-c) are the same as Fig. 4.1, but for the zonal wind at 300 hPa. (d) is the meridional cross-section of the zonal wind, from 10°-70°N latitude and averaged across 80°-120°W longitude, for the control SST. (e) and (f) are the anomalies in response to the warm and cold SST anomalies, respectively. Units are m s^{-1}.

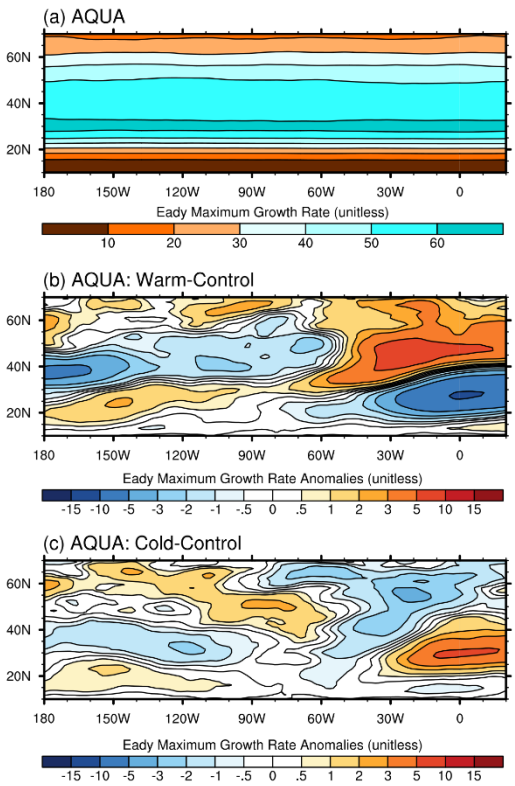

Figure 4.4: Same as Fig.4.1, but for the Eady maximum growth rate between 925 hPa and 250 hPa. The Eady growth rate is unitless. Scaling is 10^{-7}.

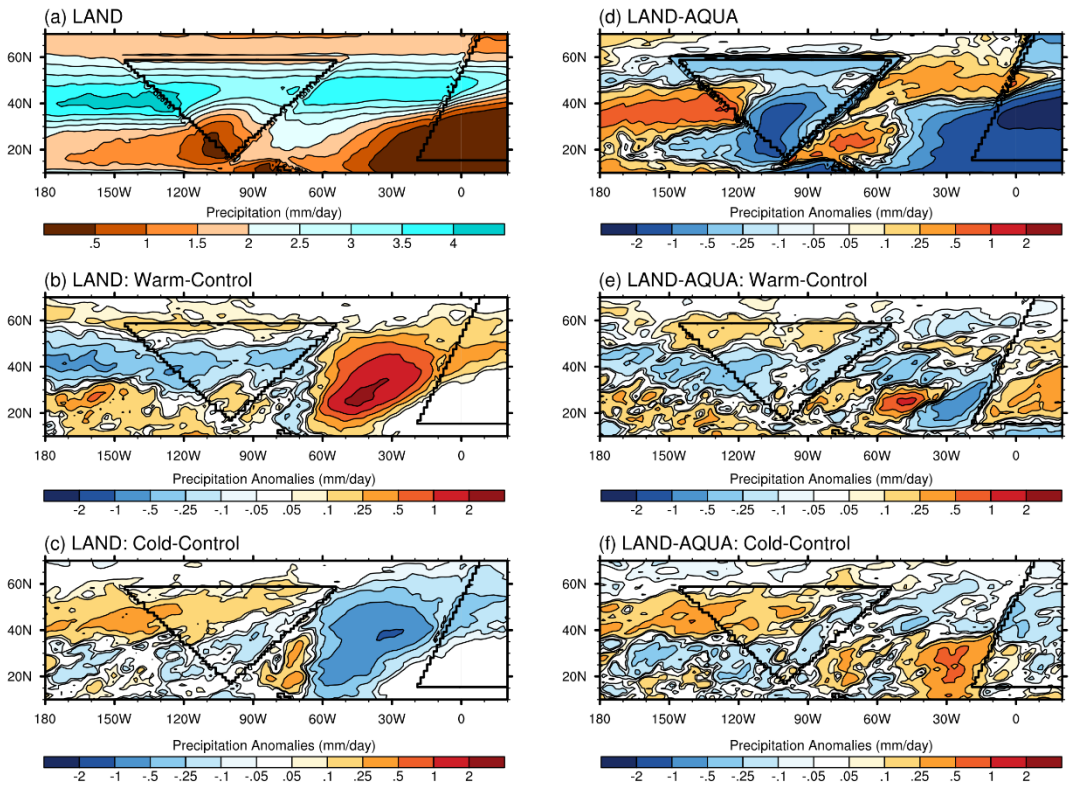

Figure 4.5: (a-c) are the same as Fig. 4.1, but for the land experiments, and (d-f) are the differences between the land experiments and the aqua-planet experiments. Units are mm day^{-1}. Note that this figure uses the more restricted domain from 10°N-70°N latitude and 180°W-20°E longitude

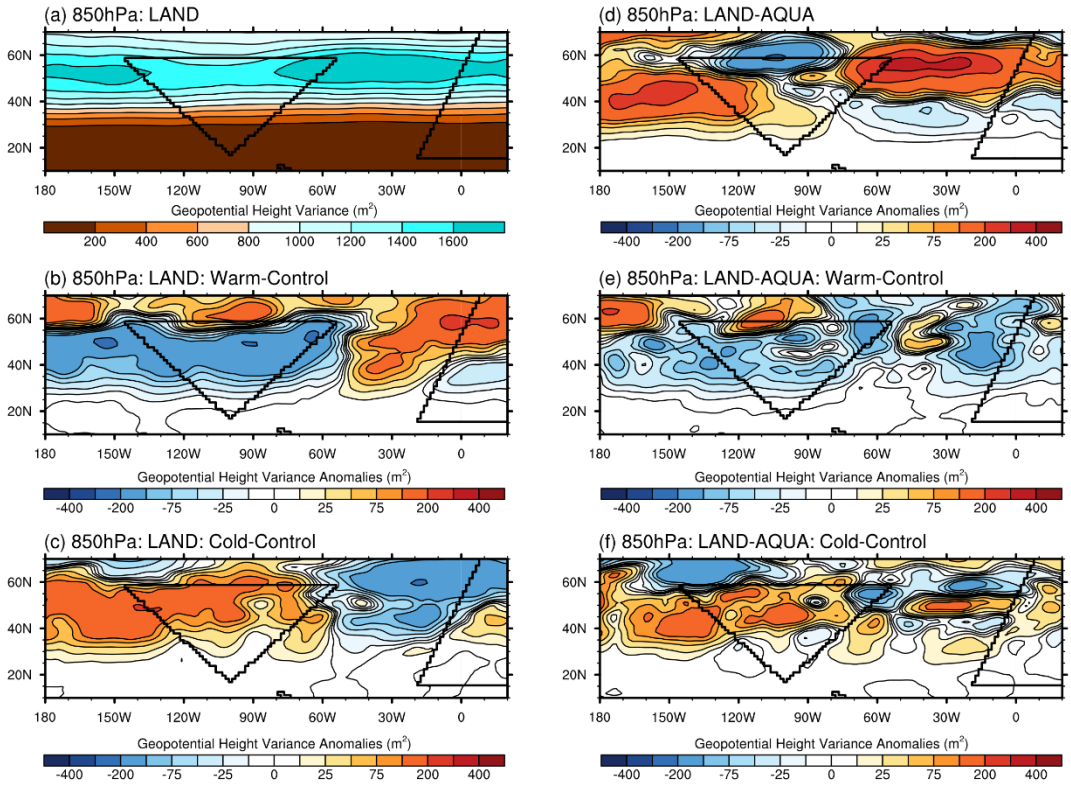

Figure 4.6: (a-c) are the same as Fig. 4.2, but for the land experiments, and (d-f) are the differences between the land experiments and the aqua-planet experiments. Units are m^2.

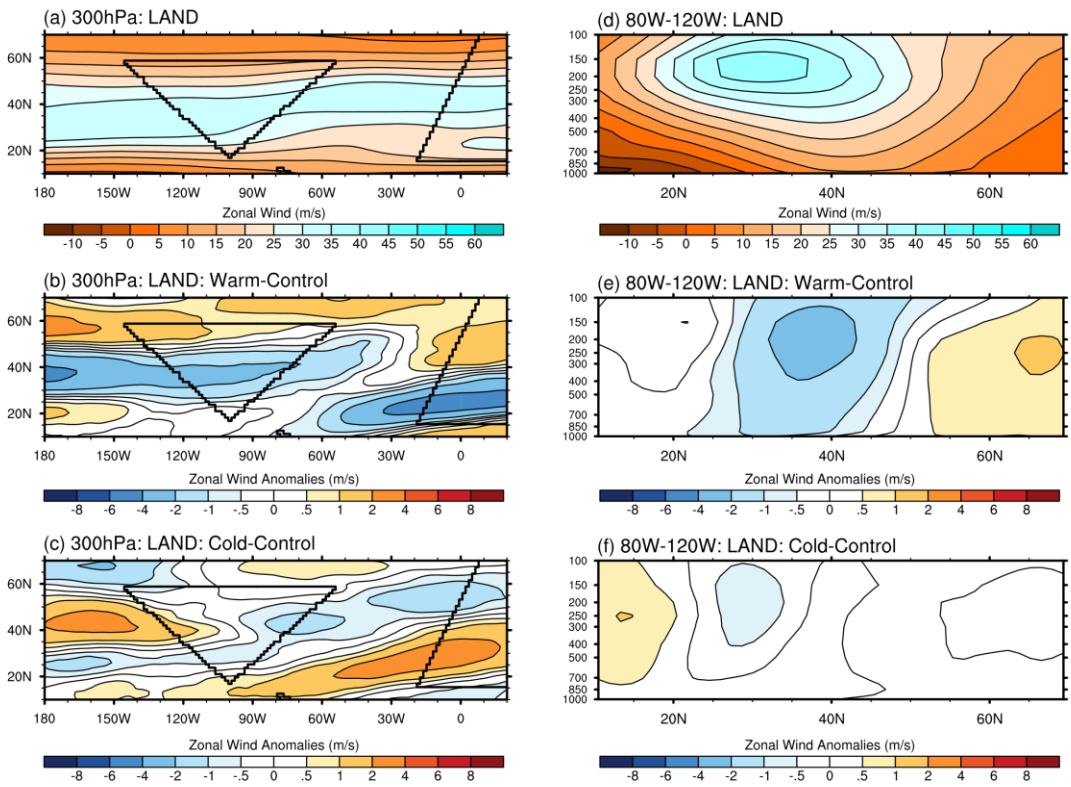

Figure 4.7: Same as Fig. 4.3, but for the land experiments. Units are m s^{-1}.

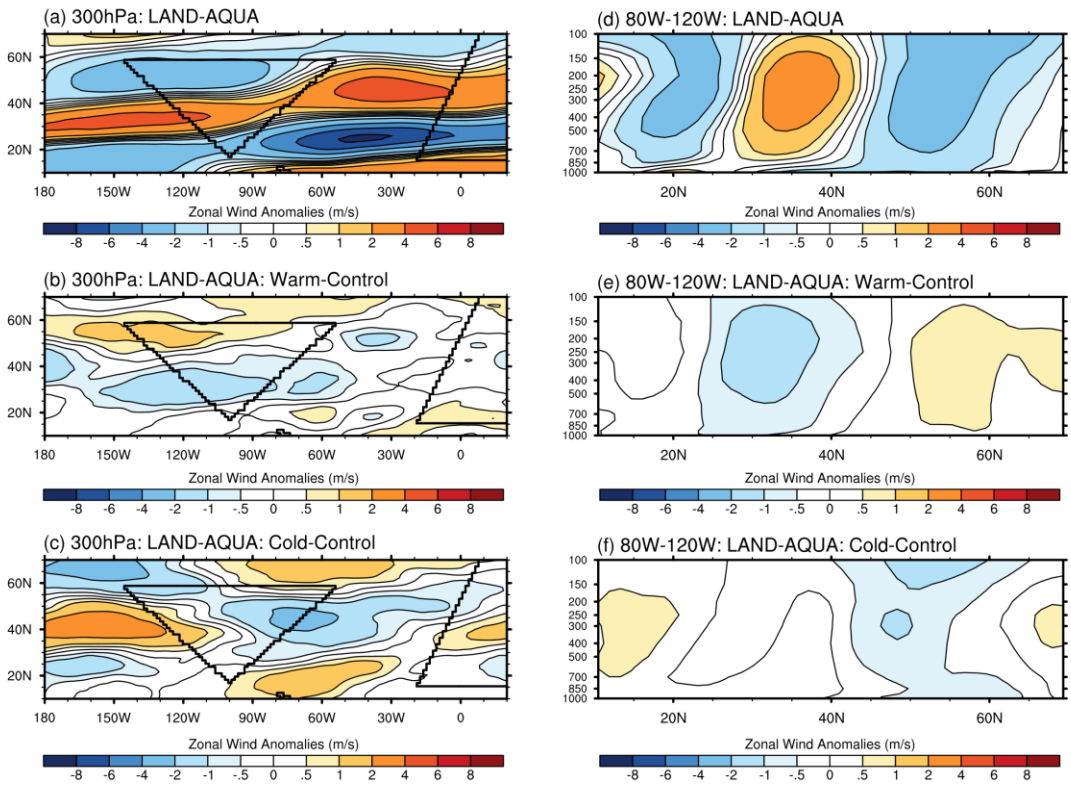

Figure 4.8: Same as Fig. 4.7, but for the difference between the land experiments and the aqua-planet experiments. Units are m s^{-1}.

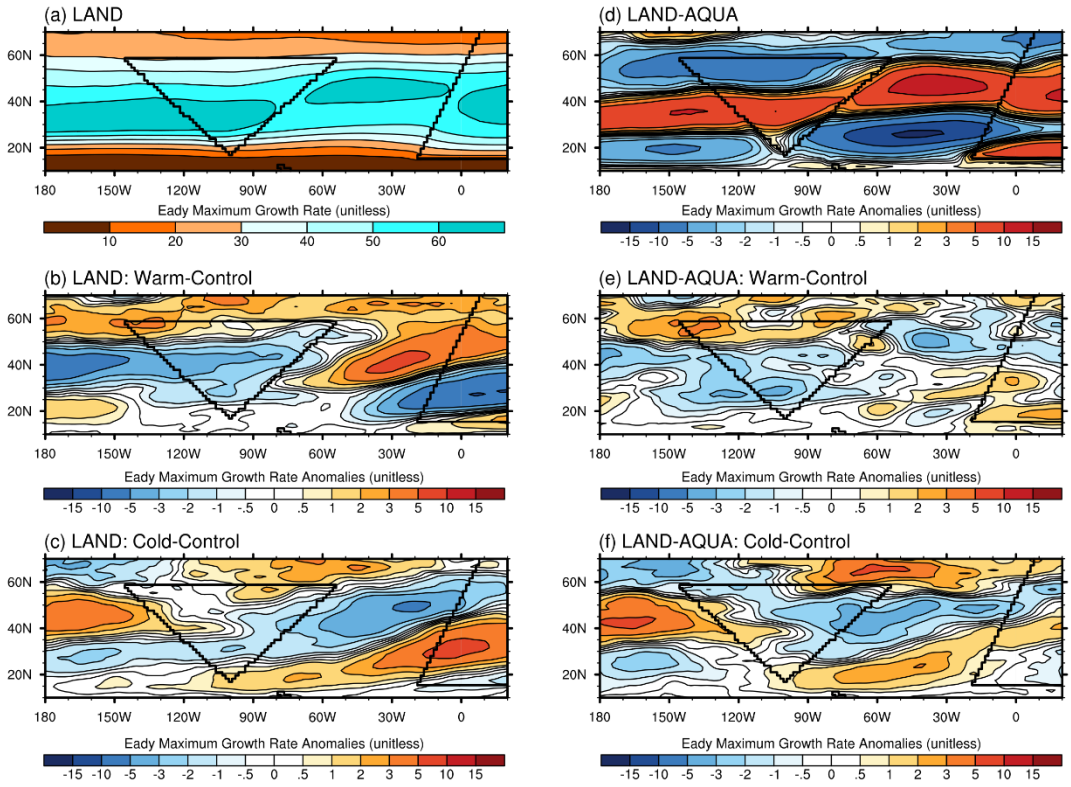

Figure 4.9: (a-c) are the same as Fig. 4.4, but for the land experiments, and (d-f) are the differences between the land experiments and the aqua-planet experiments. Scaling is 10^{-7}.

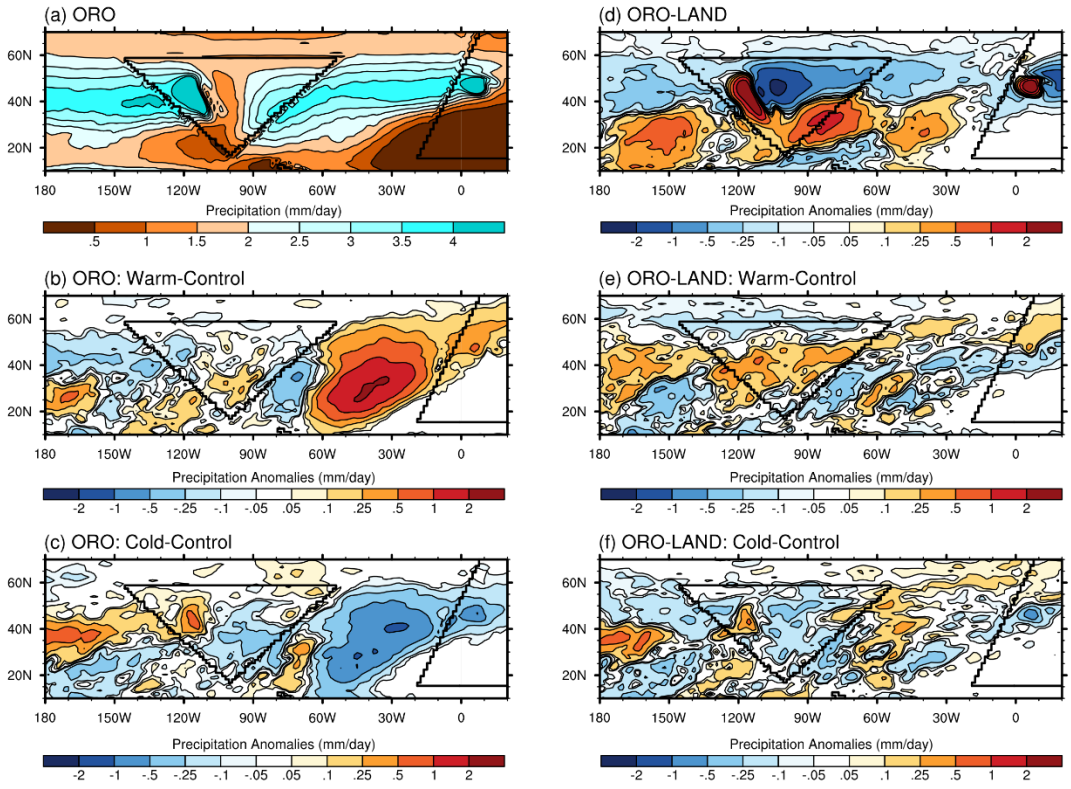

Figure 4.10: Same as Fig. 4.5, but for the orography experiments. (a-c) are the same as Fig. 4.5a-c, except for the orography experiments, and (d-f) are the differences between the land experiments and orography experiments. Units are mm day^{-1}.

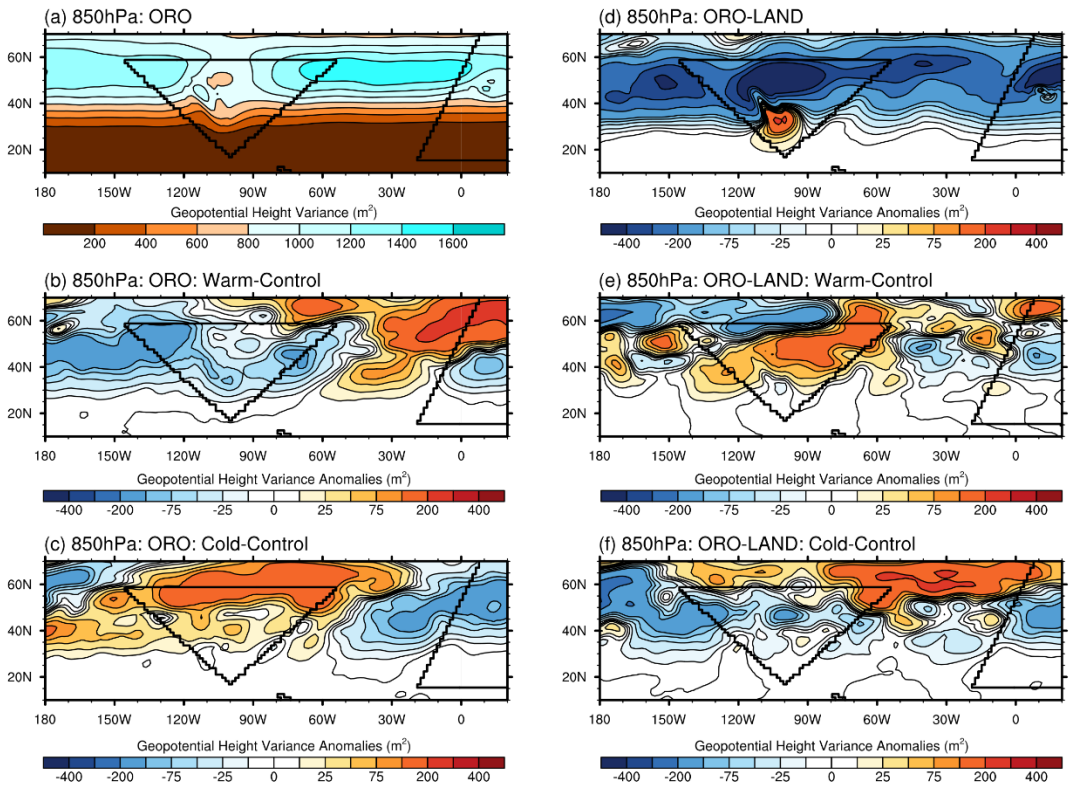

Figure 4.11: Same as Fig. 4.6, but for the orography experiments. (a-c) are the same as Fig. 4.6a-c, except for the orography experiments, and (d-f) are the differences between the land experiments and orography experiments. Units are m^2.

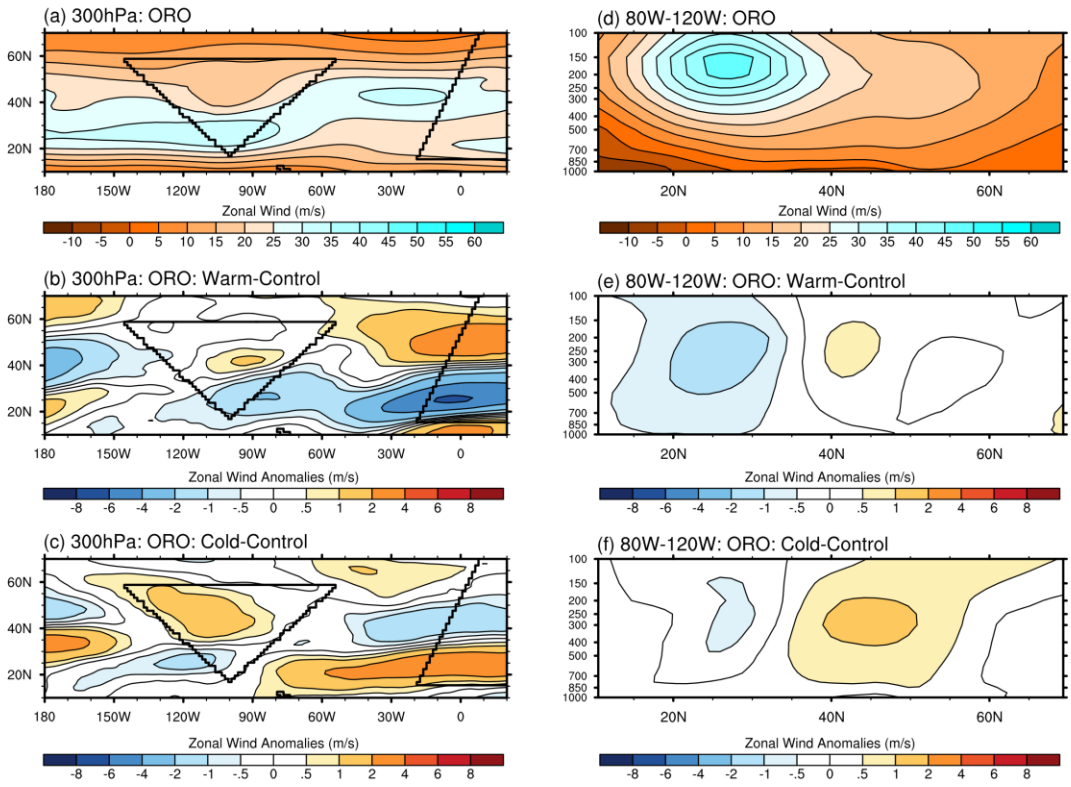

Figure 4.12: Same as Fig. 4.3, but for the orography experiments. Units are m s^{-1}.

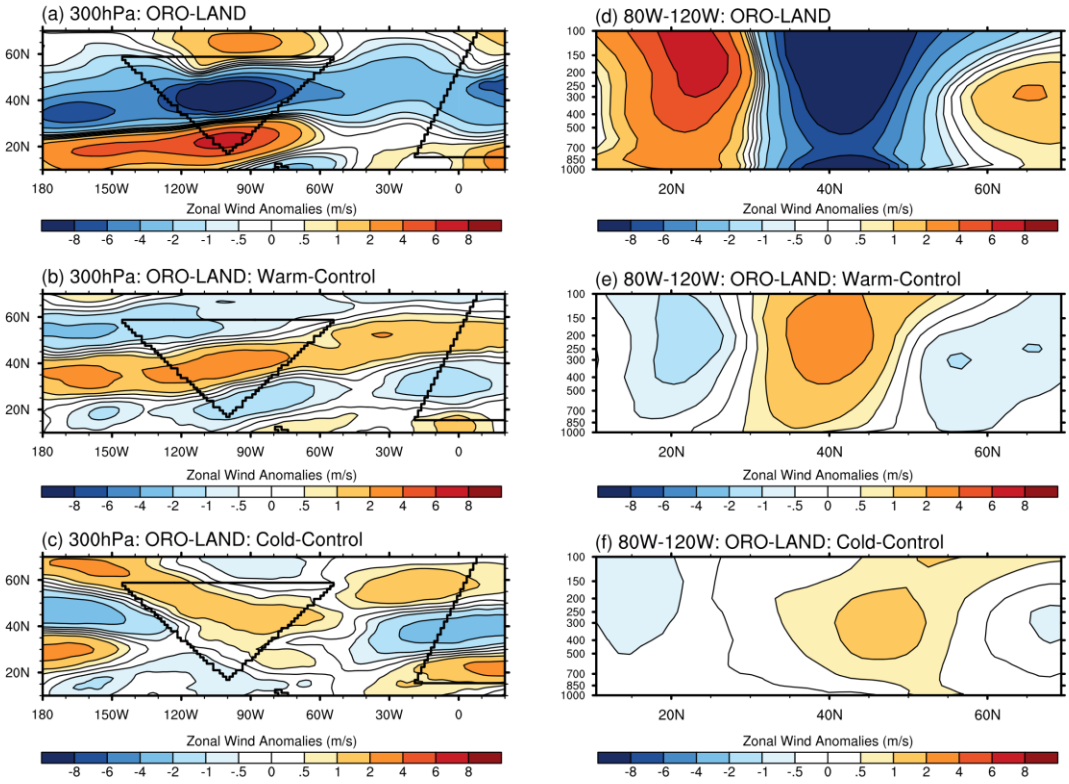

Figure 4.13: Same as Fig. 4.8, but for the differences between the orography experiments and land experiments. Units are m s^{-1}.

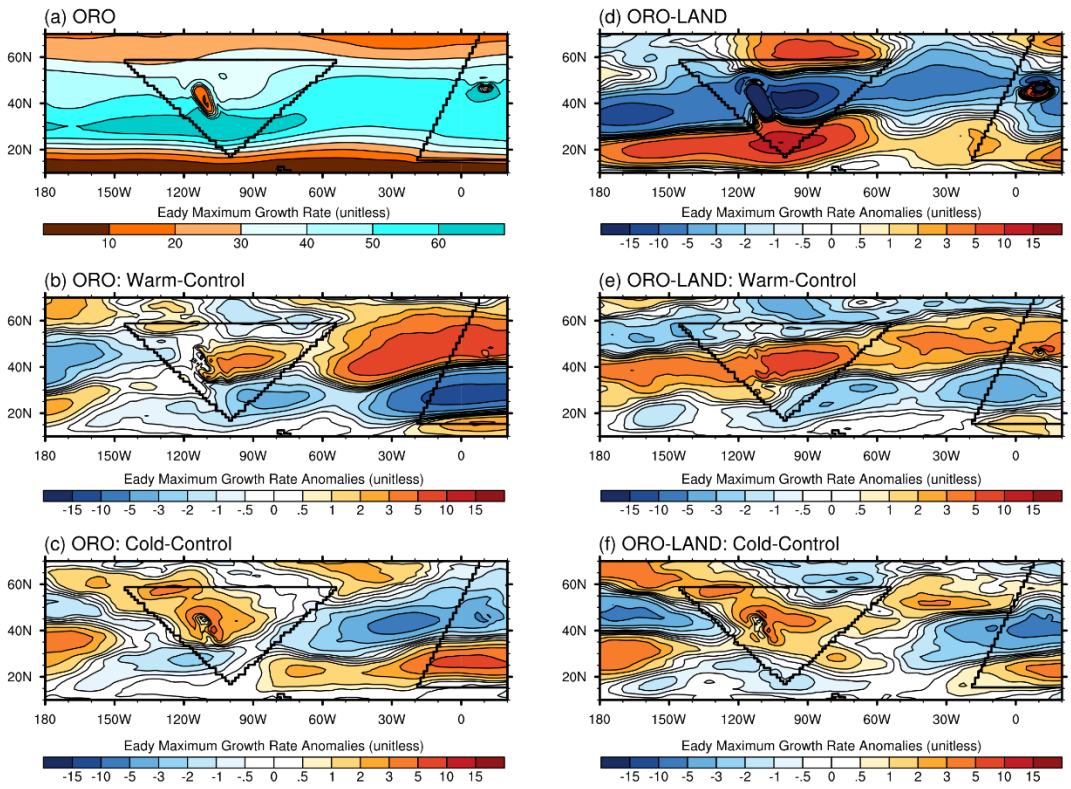

Figure 4.14: Same as Fig. 4.9, but for the orography experiments. (a-c) are the same as Fig. 4.9a-c, except for the orography experiments, and (d-f) are the differences between the land experiments and orography experiments. Scaling is 10^{-7}.

CHAPTER 5

DISCUSSION AND FUTURE WORK

This study has shown that land and orography are each critical in shaping the observed springtime circulation and precipitation responses to the SST anomalies in the North Atlantic Ocean. This is especially true upstream of the North Atlantic with the cold SST anomaly. With the warm SST anomaly, the response is less dependent upon the presence of land, but orography still significantly alters the direct response to the warm SST anomaly (from the aqua-planet experiment). In both the warm and cold SST anomaly cases, orography is largely responsible for determining the weak springtime precipitation anomalies over North America. The direct response to the SST forcing and the changes forced by land are nearly canceled by the effects of orography. Therefore, it is clear that the overall responses to the North Atlantic SST anomaly are actually the result of complex interactions between land, orography and the North Atlantic SST anomalies, and not solely forced directly by the North Atlantic SST anomalies.

The strong importance of land and orography on shaping the response to the warm and cold SST anomalies of the AMO suggest that any changes to the topographic forcings can alter the response to the AMO. As discussed in Chapter 1, Ringler and Cook (1999) suggested that topographic forcings can be variable, due to changes in land surface conditions such as land surface type and vegetation, on interannual timescales. When we combine this idea with the results of this study, it appears that any variations in the land surface forced by other local or remote factors (at interannual and decadal timescales) can influence how the atmospheric response to the AMO can be altered by

land and orography. Due to the strong magnitude and opposing nature of the land and orographic effects on both the atmospheric circulation and precipitation, we can see that any changes in the magnitudes of these effects could potentially have extensive impacts.

As a hypothetical example: Say that in certain years, the land surface conditions are such that the land modification of the circulation is weakened and hence precipitation may be changed. This could be due to changes in vegetation, snow cover (and snow melt), soil moisture or other factors. From the previous two chapters, we know that during the spring, the effect of land is quite large during the cold phase of the AMO. Therefore, we can surmise that the cold phase of the AMO may be particularly vulnerable to variations in the land forcing. With a reduced land effect, the orographic effect would become dominant (assuming no change) in the combined forcings. This rebalancing of the forcings could lead to drier conditions in the interior of North America during the AMO cold phase. A similar effect could occur with an enhancement of the orographic effect, though the possibilities are more limited. In contrast, an enhancement of the land effect or weakening of the orographic effect could lead to an increase in precipitation in the interior of North America. During the warm phase of the AMO, the land effect is relatively small compared to the direct SST forcing. However, the orographic effect is large and suggests that variations in this would be more likely to alter North American circulation and precipitation than changes in the land effect. As such, the response to a warm North Atlantic SST is likely less variable and less susceptible to change than the response to the cold SST anomaly.

Although, care must be taken when comparing the springtime results of this study to the summertime results of others, we can nonetheless begin to understand the relatively

inconsistent responses to the cold phase of the AMO compared to the warm phase of the AMO during summer (e.g., Hu et al. 2011). The direct circulation and precipitation responses to the cold phase of the AMO are quite weak upstream of the North Atlantic. When combined with any potential alterations to land and orographic forcings, there is a potential for a weak and/or inconsistent response from year-to-year. This is not the case during the warm phase of the AMO. In this case, the direct atmospheric response is strong and the only major source of variability is from the orographic effect, suggesting a stronger and less variable atmospheric response. It is this difference in importance between the three major forcings that can lead to a stronger response over North America during the warm phase of the AMO, and a weaker and more variable response during the cold phase of the AMO.

With this better understanding of the relative importance of each forcing, and how they interact, we can also examine implications of these results. One possibility is for better forecasting and predictions of inter-seasonal variability of the AMO. If changes in the land surface forced by other processes (e.g., ENSO, PDO) can be predicted for a forthcoming season, it may be possible (after additional research) to determine the relative strength of the topographic effects on the AMO response. In other words, will the topographic effects be modified, and will there be a resulting change in the circulation and precipitation as a result. Land surface changes due to a continuing phase of the AMO can also be taken into account. However, we are not yet at the point that forecasts can be made better by this information. A better understanding of how *specific* land surface changes alter the land and orographic modifications to the AMO is needed. Therefore, the next step is to determine the changes in the topographic effects under

different land cover distributions. Once these are better understood, it may become possible to connect this study to those done regarding other remote and local forcings, and allow for better interannual and inter-seasonal predictability of the responses to the warm and cold phases of the AMO.

There are different approaches that can be taken to this end. One method is by running the experiments in this study again, but with different land surface types (e.g., forest, bare ground, etc.) or introducing surface heterogeneities (multiple land surface types). By comparing these new responses to the ones presented in this study, it may be possible to determine how different land surface types may fundamentally alter the land or orography effects. Another possibility, one that is more closely applicable to reality, is to perform the experiments using more realistic topography, but also with idealized land surface coverage. Using the results of the current study as a starting point, it may be possible to examine the impact of interannual land surface changes and their role on modifying the response to the AMO year-to-year. In these experiments, it would be possible to skip the aqua-planet and land without orography surface boundaries. Either of these experiment designs could potentially provide new information regarding the role of land surface conditions on the interannual variability of the AMO, a topic that has not been discussed much in the literature, but has been shown by the current study to possibly be important in shaping the response to the AMO.

Understanding the changes in the land and orography effects can have further implications if we consider future climate change scenarios. Overpeck et al. (1990) suggested that a warming climate would lead to changes in the land cover distribution. From our previous discussion, we can see that changes in the land surface forced by

global warming has the potential to alter the land effects in response to the AMO. While any extrapolation of these results to climate change scenarios must be made cautiously, as the AMO itself may be altered from a change in the Atlantic Meridional Overturning Circulation (AMOC; Zickfield et al. 2007 and references therein), it may be possible to get an initial idea as to how the atmospheric response to the AMO may change, and what may drive those potential changes. However, as with the seasonal and interannual predictions just discussed, a more detailed analysis of the way in which the land and orographic effects can vary in response to land surface changes is needed.

In conclusion, this study has demonstrated that the atmospheric response to the AMO is quite complex. By splitting the SST, land and orographic forcings apart, we have been able to obtain a better idea as to how the AMO forces changes in the springtime circulation and precipitation. What we found is that the total response to the warm phase of the AMO is largely determined by the SST forcing, and the orographic modification of this response. In contrast, the direct response to the cold phase of the AMO is fairly weak and is heavily modified by both land and orography. Furthermore, the potential impacts of land surface variations have been identified, and strongly suggest additional work for the future in order to more fully understand and predict the circulation and precipitation anomalies induced by the AMO.

REFERENCES

Blackburn, M., and coauthors, 2013: The Aqua-Planet Experiment (APE): CONTROL SST simulation, *J. Meteor. Soc. Japan*, **91A**, 17-56.

Brayshaw, D.J., B. Hoskins and M. Blackburn, 2008: The storm-track response to idealized SST perturbations in an aquaplanet GCM. *J. Atmos. Sci.*, **65**, 2842-2860.

Brayshaw, D.J., B. Hoskins and M. Blackburn, 2009: The basic ingredients of the North Atlantic storm track. Part I: Land-sea contrast and orography. *J. Atmos. Sci.*, **66**, 2539-2558.

Brayshaw, D.J., B. Hoskins and M. Blackburn, 2011: The basic ingredients of the North Atlantic storm track. Part II: Sea surface temperatures. *J. Atmos. Sci.*, **68**, 1784-1805.

Breshears, D.B., and coauthors, 2005: Regional vegetation die-off in response to global-change-type drought. *Proc. Natl. Acad. Sci. USA*, **102**, 15144-15148.

Broccoli, A.J., and S. Manabe, 1992: The effects of orography on Midlatitude Northern Hemisphere dry climates. *J. Climate*, **5**, 1181-1201.

Chang, E., S. Lee and K.L. Swanson, 2002: Storm track dynamics. *J. Climate*, **15**, 2163-2183.

Charney, J.G., 1947: The dynamics of long waves in a baroclinic westerly current. *J. Meteor.*, **4**, 135-162.

Chase, T., R. Pielke Sr., T. Kittel, J. Baron and T. Stohlgren, 1999: Potential impacts on Colorado Rocky Mountain weather due to land use changes on the adjacent Great Plains, *J. Geophys. Res.*, **104**, 16,673-16690.

Davis, R.E., B.P. Hayden, D.A. Gay, W.L. Phillips, and G.V. Jones, 1997: The North Atlantic subtropical anticyclone, *J. Climate*, **10**, 728-744.

Derome, J., and A. Wiin-Nielsen, 1971: The response of a middle-latitude model atmosphere to forcing by topography and stationary heat sources. *Mon. Wea. Rev.*, **99**, 564-576.

Eady, E., 1949: Long waves and cyclone waves. *Tellus*, **1**, 33-52.

Enfield, D.B., A.M. Mestas-Nuñez and P.J. Trimble, 2001: The Atlantic Multidecadal Oscillation and its relation to rainfall and river flows in the Continental U.S. *Geophys. Res. Lett.*, **28**, 2077-2080.

Feng, S., and Q. Hu, 2008: How the North Atlantic Multidecadal Oscillation may have influenced the Indian summer monsoon during the past two millennia. *Geophys. Res. Lett.*, **35**, L01707.

Feng, S., Q. Hu, and R.J. Oglesby, 2010: Influence of Atlantic sea surface temperatures on persistent drought in North America. *Climate Dynamics*, **37**, 569-586.

Gray, S.T., L.J. Graumlich, J.L. Betancourt, and G.T. Pederson, 2004: A tree-ring based reconstruction for the Atlantic Multidecadal Oscillation since 1567 A.D., *Geophys. Res. Lett.*, **31**, L12205.

Higgins, R.W., Y. Yao, E.S. Yarosh, J.E. Janowiak, and K.C. Mo, 1997: Influence of the Great Plains low-level jet on summertime precipitation and moisture transport over the Central United States. *J. Climate*, **10**, 481-507.

Hoskins, B.J. and D.J. Karoly, 1981: The steady linear response of a spherical atmosphere to thermal and orographic forcing. *J. Atmos. Sci.*, **38**, 1179-1196.

Hoskins, B.J. and P.J. Valdes, 1990: On the existence of storm-tracks, *J. Atmos. Sci.*, **47**, 1854-1864.

Hu, Q., and S. Feng, 2001: Variations of teleconnection of ENSO and interannual variation in summer rainfall in the Central United States. *J. Climate*, **14**, 2469-2480.

Hu, Q., and S. Feng, 2008: Variation of the North American summer monsoon regimes and the Atlantic Multidecadal Oscillation, *J. Climate*, **21**, 2371-2383.

Hu, Q. and S. Feng, 2012: AMO- and ENSO-driven summertime circulation and precipitation variations in North America. *J. Climate*, **25**, 6477-6495.

Hu, Q., S. Feng and R. Oglesby, 2011: Variations in North American summer precipitation driven by the Atlantic Multidecadal Oscillation. *J. Climate*, **24**, 5555-5570.

Hurrell, J.W., and coauthors, 2013: The Community Earth System Model: A framework for collaborative research, *Bull. Amer. Meteor. Soc.*, **94**, 1339-1360.

Keyser, D. and R.A. Anthes, 1982: An alternative expression for the Eady wave growth rate, *J. Atmos. Sci.*, **39**, 1877-1881.

Liu, Y., G. Wu, and R. Ren, 2004: Relationship between the subtropical anticyclone and diabatic heating, *J. Climate*, **17**, 682-698.

McCabe, G.J., M.A. Palecki, and J.L. Betancourt, 2004: Pacific and Atlantic Ocean influences on multidecadal drought frequency in the United States, *Proc. Natl. Acad. Sci. USA*, **101**, 4136-4141.

Mo, K.C., J.E. Schemm, and S. Yoo, 2009: Influence of ENSO and the Atlantic Multidecadal Oscillation on drought over the United States, *J. Climate*, **22**, 5962-5982.

Neale, R.B. and Hoskins, B.J., 2000: A standard test for AGCMs including their physical parameterizations: I: The proposal. *Atmos. Sci. Lett.*, **1**, 101-107.

Nakamura, H., T. Sampe, Y. Tanimoto and A. Shimpo, 2004: Observed associations among storm tracks, jet streams and midlatitude oceanic fronts, *Earth's Climate: The Ocean-Atmosphere Interaction, Geophys. Monogr*, No. 147, Amer. Geophys. Union, 329-345.

Newton, C.W., 1979: Mountain torques in the global angular momentum balance. *J. Atmos. Sci.*, **28**, 623-628.

Nigam S., B. Guan and A. Ruiz-Barradas, 2011: Key role of the Atlantic Multidecadal Oscillation in 20th century drought and wet periods over the Great Plains. *Geophys. Res. Lett.*, **38**, L16713.

Oglesby, R.J., and D.J. Erickson III, 1989: Soil moisture and the persistence of North American drought, *J. Climate*, **2**, 1362-1380.

Oglesby, R.J., S. Marshall, J.O. Roads, and F.R. Robertson, 2001: Diagnosing warm season precipitation over the GCIP region from a GCM and reanalysis. *J. Geophys. Res.*, **106**, 3357-3369.

Overpeck, J.T., D. Rind, and R. Goldberg, 1990: Climate-induced changes in forest disturbance and vegetation, *Nature*, **343**, 49-51.

Peixoto, J.P., and A.H. Oort, 1992: *Physics of Climate*. American Institute of Physics, 520 pp.

Pielke, R., G. Dalu, J. Snook, T. Lee and T. Kittel, 1991: Nonlinear influence of mesoscale land use on weather and climate. *J. Climate*, **4**, 1053-1069.

Pielke Sr., R.J., 2001: Influence of the spatial distribution of vegetation and soils on the prediction of cumulus convective rainfall. *Rev. Geophys.*, **39**, 151-177.

Pielke Sr., R., Adegoke, A. Beltrán-Przekurat, C. Hiemstra, J. Lin, U. Nair, D. Niyogi and T. Nobis, 2007: An overview of regional land-use and land-cover impacts on rainfall. *Tellus*, **59B**, 587-601.

Poore, R.Z., K.L. DeLong, J.N. Richey, and T.M. Quinn, 2009: Evidence of multidecadal climate variability and the Atlantic Multidecadal Oscillation from a Gulf of Mexico sea-surface temperature-proxy, *Geo-Marine Lett.*, **29**, 477-484.

Rayner, N.A., P. Brohan, D.E. Parker, C.K. Folland, J.J. Kennedy, M. Vanicek, T. Ansell, and S.F. B.Tett, 2006: Improved analyses of changes and uncertainties in sea surface temperature measured in situ since the mid-nineteenth century: the HadSST2 data set. *J.* Climate, **19**, 446-469.

Ringler, T.D. and K.H. Cook, 1999: Understanding the seasonality of orographically forced stationary waves: Interaction between mechanical and thermal forcing. *J. Atmos. Sci.*, **56**, 1154-1174.

Rodwell, M.J., and B.J. Hoskins, 2001: Subtropical anticyclones and summer monsoons, *J. Climate*, **14**, 3192-3211.

Schubert, S., and coauthors, 2009: A U.S. CLIVAR project to assess and compare the responses of global climate models to drought-related SST forcing patterns: overview and results. *J. Climate*, **22**, 5251-5272.

Schubert, S.D., M.J. Suarez, P.J. Pegion, R.D. Koster, and J.T. Bachmeister, 2004: Causes of long-term drought in the U.S. Great Plains. *J. Climate*, **17**, 485-503.

Seager, R., R. Murtugudde, N. Naik, A. Clement, N. Gordon, and J. Miller, 2003: Air-sea interaction and the seasonal cycle of the subtropical anticyclones, *J. Climate.*, **16**, 1948-1966.

Sutton, R.T., and B. Dong, 2012: Atlantic Ocean influence on a shift in European climates in the 1990s. *Nature Geosci.*, **5**, 788-792.

Sutton, R.T., and D.L.R. Hodson, 2005: Atlantic Ocean forcing of North American and European summer climate. *Science*, **309**, 115-118.

Ting, M., 1994: Maintenance of northern summer stationary waves in a GCM. *J. Atmos. Sci.*, **51**, 3286-3308.

Ting, M., and H. Wang, 1997: Summertime U.S. precipitation variability and its relation to Pacific sea surface temperature. *J. Climate*, **10**, 1853-1873.

Ting, M., and H. Wang, 2006: The role of the North American topography on the maintenance of the Great Plains summer low-level jet, *J. Atmos. Sci.*, **63**, 1056-1068.

Veres, M.C., and Q. Hu, 2013: AMO-forced regional processes affecting summertime precipitation variations in the central United States. *J. Climate*, **26**, 276-290.

Wallace, J.M., and D.S. Gutzler, 1981: Teleconnections in the geopotential height field during the Northern Hemisphere winter, *Mon. Wea. Rev.*, **109**, 784-812.

Wang, S., and T. Chen, 2009: The late-spring maximum of rainfall over the U.S. Central Plains and the role of the low-level jet. *J. Climate*, **22**, 4696-4709.

Wang, H., S. Schubert, M. Suarez and R. Koster, 2010: The physical mechanisms by which the leading patterns of SST variability impact U.S. precipitation. *J. Climate*, **23**, 1815-1836.

Wang, C., and L. Zhang, 2013: Multidecadal ocean temperature and salinity variability in the tropical North Atlantic: Linking with the AMO, AMOC, and subtropical cell. *J. Climate*, **26**, 6137-6162.

Weaver, S.J. and S. Nigam, 2008: Variability of the Great Plains low-level jet: Large-scale circulation context and hydroclimate impacts. *J. Climate*, **21**, 1532-1551.

Webster, P.J., 1981: Mechanisms determining the atmospheric response to sea surface temperature anomalies. *J. Atmos. Sci.*, **38**, 554-571.

Webster, P.J., 1982: Seasonality in the local and remote atmospheric response to sea surface temperature anomalies, *J. Atmos. Sci.*, **39**, 41-52.

White, R.M., 1949: The role of mountains in the angular-momentum balance of the atmosphere. *J. Meteor.*, **6**, 353-355.

Zickfield, K., A. Levermann, M.G. Morgan, T. Kuhlbrodt, S. Rahmstorf, and D.W. Keith, 2007: Expert judgements on the response of the Atlantic meridional overturning circulation to climate change. *Climatic Change*, **82**, 235-265.